2015

Determining the Efficacy of Magnetic Susceptibility as an Analytical Tool in the Middle Devonian Gas Bearing Shale of Taylor County, West Virginia

John Baird

Determining the Efficacy of Magnetic Susceptibility as an Analytical Tool in the Middle Devonian Gas Bearing Shale of Taylor County, West Virginia

John Baird

Thesis submitted to the
Eberly College of Arts and Sciences
at West Virginia University

in partial fulfillment of the requirements
for the degree of

Masters of Science in
Geology

Timothy Carr, PhD., Chair
Ryan Shackleton, PhD.
Shikha Sharma, PhD.

Department of Geology and Geography

Morgantown, West Virginia
2015

Keywords: Marcellus Shale, Mahantango Formation, Magnetic Susceptibility, Organic Carbon, Sequence Stratigraphy, Brittleness, Kerogen, Petrophysics

Abstract

Determining the Efficacy of Magnetic Susceptibility as an Analytical Tool in the Middle Devonian Gas Bearing Shale of Taylor County, West Virginia

John Baird

The magnetic susceptibility of two Middle Devonian shale units, the Mahantango Formation and Marcellus Shale, was recorded in order to determine if magnetic susceptibility could be used to predict (1) transgressive and regressive cycles, (2) brittleness, and (3) total organic content (TOC). A core from Taylor County, West Virginia was selected for this purpose.

Transgressive and regressive cycles were detected through variations of magnetic susceptibility values with maximum flooding surfaces indicated by troughs in the data and maximum regressive surfaces indicated by peaks. A sequence stratigraphic framework based upon variations in gamma ray and density measurements was used to establish a standard to gauge the accuracy of predictions made through magnetic susceptibility. It was found that the accuracy of the magnetic susceptibility method was similar to the gamma-density method in detecting a large 2nd order cycle, when both shale units were evaluated together. When the units were evaluated separately, it was found that both methods detected the same 3rd order cycles. However, within the Mahantango Formation the magnetic susceptibility method was more accurate recording 4th order cycles that the gamma-density method did not. Conversely, within the Marcellus Shale, the gamma-density method was more accurate recording 4th order cycles that the magnetic susceptibility method did not. It was concluded that the increased accuracy of the gamma-density method in the Marcellus shale was due to an increased sensitivity in the gamma ray and density logs as a response to the large amounts of TOC in the formation This increased sensitivity allowed for smaller variations to be more easily detected. The Mahantango Formation does not have large quantities of TOC. This diminished the sensitivity of the gamma and density logs allowing for the magnetic susceptibility method to be more accurate.

It was assumed that variations in brittleness are driven by transgressive and regressive cycles with ductile regions coinciding with maximum flooding surfaces and brittle regions coinciding with maximum regressive surfaces. Since magnetic susceptibility is also linked to transgressive and regressive cycles, it was expected that the sequence stratigraphy established previously could be linked to brittle and ductile couplets. The sequence stratigraphy established with the gamma-density method was also tested. Two methods of calculating a brittleness index were used to establish a baseline to test against. The first was based upon mineralogy and the second was based upon elastic properties. The brittleness index based

upon mineralogy compared well to 3rd order transgressive and regressive cycle detected by both methods. Magnetic susceptibility failed to detect 4th order cycles within the Marcellus Shale, but detected 4th order cycles in the Mahantango Formation that mineralogy and elastic properties missed. The brittleness index based upon mineralogy aligns better with the sequence stratigraphy produced by the magnetic susceptibility method than with the gamma-density method. The brittleness index produced by elastic properties did not correlate with either method. Further, the brittleness index produced with elastic properties did not even correlate with the brittleness index produced by mineralogy. This disagreement cast doubt upon the effectiveness of both brittleness indices.

The relationship between magnetic susceptibility and TOC was tested along with the three most common wireline techniques in order to determine which, if any, were superior. All were judged in comparison to TOC derived from the core using Rock-Eval pyrolysis. The methods tested were: Schmoker's 1983 density equation, Schmoker's 1993 density equation, and the ΔlogR method. It was found that both the magnetic susceptibility of the whole rock and the magnetic susceptibility of its isolated kerogen component correlated better with core TOC values than any of the methods tested. The accuracy of the magnetic susceptibility of the whole rock was within the same order of magnitude as the other methods, and the accuracy of the magnetic susceptibility of the isolated kerogen component was an order of magnitude higher. In addition, evidence was found that links the magnetic susceptibility of kerogen within the two units to the composition of the kerogen. Vitrinite reflectance data confirms that variations in the magnetic susceptibility of the kerogen was not caused by variations in maturity. A very strong logarithmic relationship was found between the magnetic susceptibility of kerogen and the weight percent present. Using the hypothesis that variations in the amount of organic material present is linked to episodic algal blooms, it was concluded that the organic material supplied by these blooms significantly lowered the magnetic susceptibility of the organic sediment supplied during the normal habitat of the basin.

Contents

Introduction

Geologic Background

The study area in Taylor County, West Virginia is located in the north-central part of the state and is within the Appalachian basin (Figure 1). The Middle Devonian shale units are contained within the Hamilton Group and consist of the Marcellus Shale and Mahantango Formation (Figure 2). The Hamilton Group was deposited in a restricted foreland basin formed by down warping of the lithosphere due to isostatic compensation during the formation of a mountain chain during the Acadian orogeny (Castle, 2001). At the time of orogeny, the area was located near the equator with the mountain range running east-west and the basin to the north. Due to its location, easterly trade winds are interpreted to be blocked from the south creating an orographic effect to the north resulting in sediment starvation (Ettensohn and Barron, 1981). When sediment starvation is coupled with high rates of organic production, large amounts of

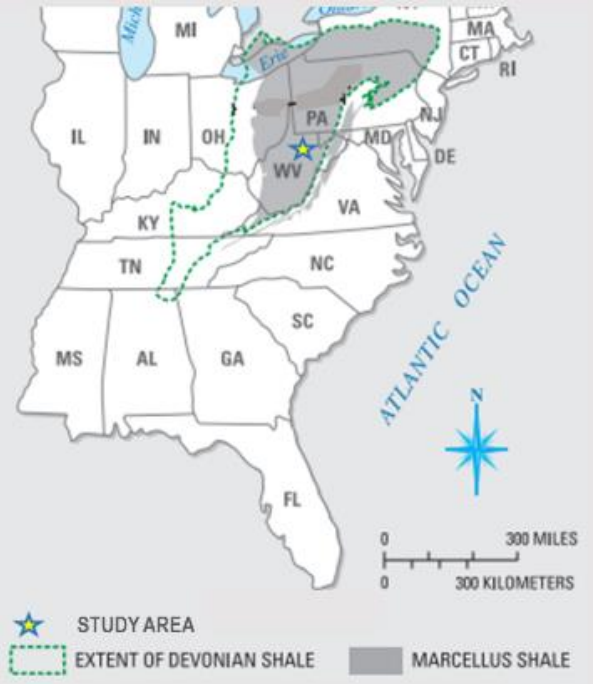

Figure 1. Extent of the Devonian shale in the Appalachian basin and location of the study area. Modified from Milici & Swezey, (2006).

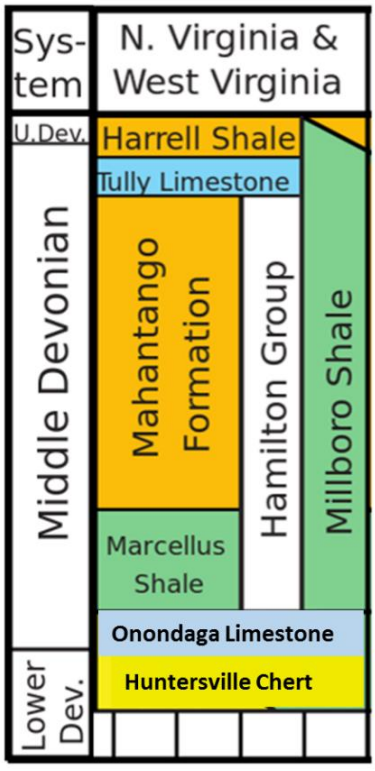

Figure 2. Stratigraphic column of the Middle Devonian in the northern Appalachian basin. Shale units consist of the Mahantango Formation and Marcellus shale. After Milici and Swezey (2006).

organic carbon can be preserved.

Magnetic Susceptibility

Magnetic susceptibility is a measure of how easily or difficult it is to magnetize a substance. The susceptibility of a material can be measured by the introduction of a magnetic field. This field affects the way electrons spin and therefore alters the direction of the magnetic field they produce. This induced change in the magnetic field in turn affects the applied field and it is this change that is measured (Ellwood, 2000). The event is expressed as a ratio:

$$\kappa = \frac{M}{H}$$

Where M is the induced magnetic field expressed in amperes/meter, H is the applied magnetic field expressed in amperes/meter, and κ (Kappa) is the resulting dimensionless measure of volume susceptibility and expressed as SI (Rochette, 1992).

When a substance has unpaired electrons in the valence shell, their spins are unrestricted. This allows the electrons to alter their spins to align with the applied magnetic field (H). When this occurs, the induced field (M) increases the strength of the applied field and produces a positive susceptibility value (Figure 3). When the valence shell is full, magnetic fields produced by each electron pair are canceled due to their opposing spins. This restricts the electrons from aligning to an applied field. When a field is applied, the push and pull of these opposing fields weakens the applied field and produces a low or even negative susceptibility value (Figure 4). The same effect can also be caused by multiple layers of full shells below the valence shell.

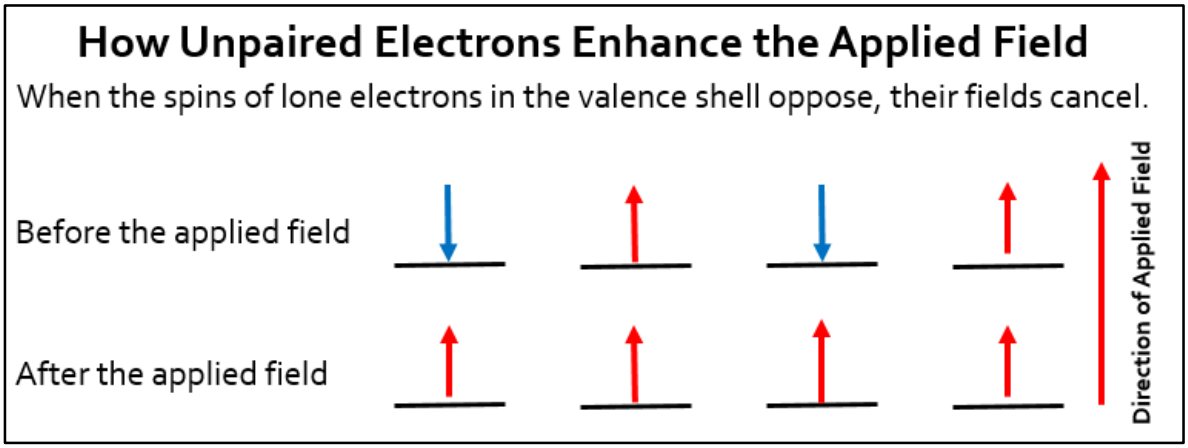

Figure 3. Unpaired electron will alter their fields to align with the applied field. When the direction of the induced field is the same as the applied field, the strength of the applied field is enhanced.

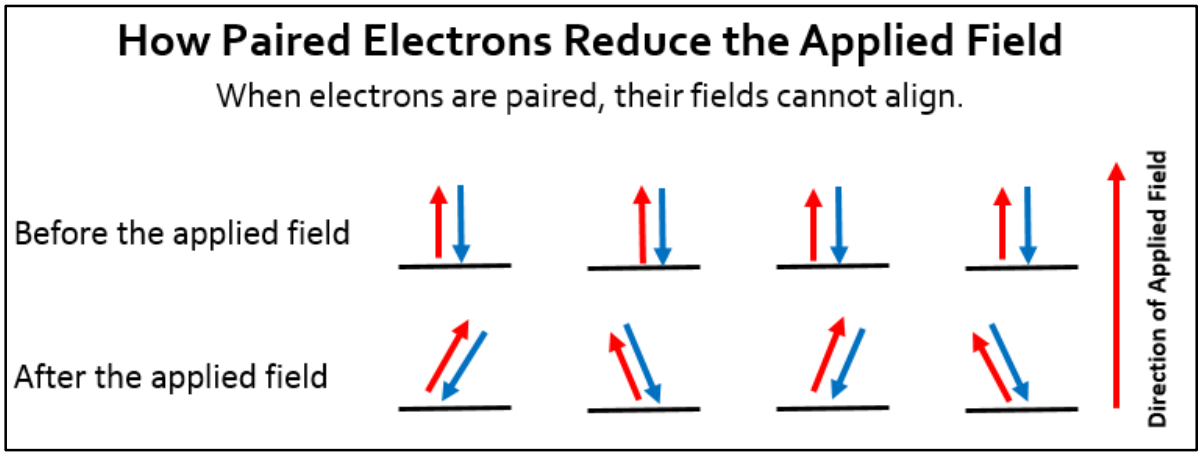

Figure 4. Paired electron spins are still altered by the applied field, but are not able to align with it. When the direction of the induced field does not align with the applied field, the strength of the applied field is reduced.

Minerals are placed into three categories based upon their susceptibility to magnetism. Those minerals that are the most susceptible are ferromagnetic minerals. Ferromagnetic minerals can produce an induced field (M) 1000 times greater than the applied field (H) and are capable of permanent magnetization (Mulay, 1963). The classic examples of ferromagnetic minerals are magnetite and hematite. Most minerals are in the remaining two categories. Minerals that produce a positive susceptibility value, but do not exhibit permanent magnetism are paramagnetic. These minerals typically contain iron. Examples include pyroxenes,

amphiboles, and biotite. Minerals that produce a negative susceptibility value are diamagnetic. Examples include calcite, quartz, and halite.

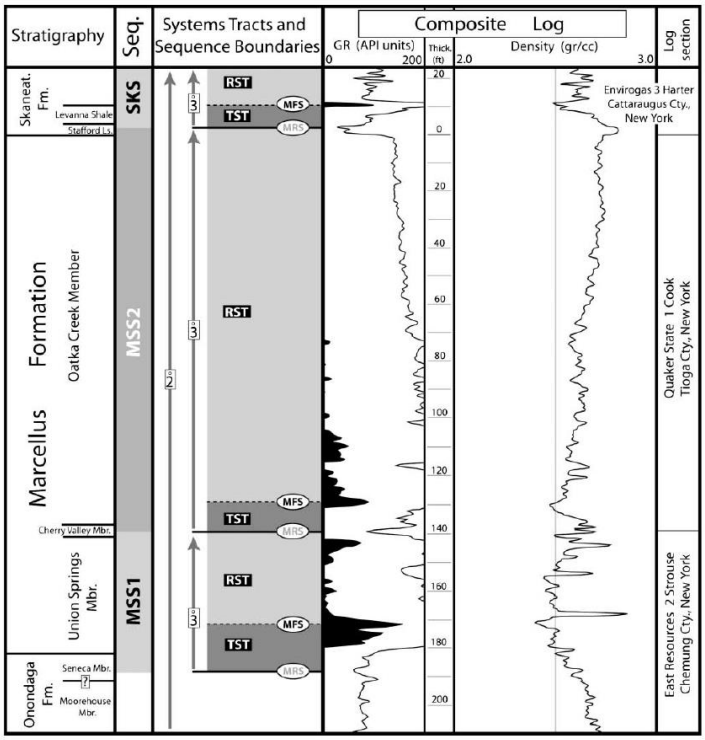

Figure 5. Sequence-stratigraphic intervals of the Marcellus Formation in south central New York. **TST**=transgressive systems tract; **RST**=regressive systems tract; **MFS**=maximum flooding surface; **MRS**=maximum regressive surface. (Lash & Engelder, 2011).

Sequence Stratigraphy

The Devonian shale records a second order transgressive-regressive (T-R) sequence with the Marcellus shale displaying two 3rd order T-R sequences and at least one other 3rd order sequence in the Mahantango Formation (Lash and Engelder, 2009) (Figure 5). A T-R sequence indicates the rise and fall of base level within the basin and is bounded by the maximum flooding surface (MFS) and maximum regressive surface (MRS). The transgressive system tract (TST) records a rise in base level and fining-upward sequence in the form of increased gamma-ray response and decreased density response. It is capped at the MFS marking the point of the greatest rise of base level in the sequence. The regressive systems tract (RST) records a fall in base level in the form of a coarsening upward sequence, decreased gamma-ray response and increased density response. It is capped by the MRS. This is the furthest that base level fell in the sequence (Figure 5).

Identifying sequences and sequence tracks aids hydrocarbon exploration due to a direct correlation between system tracts, organic-carbon levels, and rock mechanics (Slatt, 2014). As a TST approaches a MFS, the organic carbon in a basin becomes more marine and less terrestrial. This leads to more oil-prone type I and II kerogen deposition. In addition, the area of deposition becomes more distant to terrigenous grain input, resulting in more organic carbon with respect to clastic material and a higher total organic carbon (TOC) percentage. As water depth increases during the TST it creates more accommodation space, which allows for more deposition. The deeper water restricts currents and therefore oxygen creating anoxic waters conducive to the preservation of organic carbon. A direct correlation has been found between TSTs in marine source rocks and an increase of TOC (Creaney and Passey, 1993).

In sedimentary rocks, magnetic susceptibility is typically controlled by the percentage of paramagnetic grains to diamagnetic grains. Paramagnetic values are generally due to the iron content from terrigenous sediments (Nagata, 1961). Paramagnetic sediments will generally be deposited closer to shore due to their iron content, while those sediments deposited further from shore will tend to contain less iron and be more diamagnetic. The ratio of paramagnetic to diamagnetic grains in the rock can be controlled by erosion due to climate and/or changes in base level (Crick et al., 1997). Since the basin is located in an orographic rain shadow, variations in magnetic susceptibility can be attributed to changes in base level. It has been shown that, during changes in base level, the magnetic susceptibility of marine rocks decreases during transgression and increases during regression (Ellwood, 2001). During a TST, the source of terrigenous grains is further away from the area of deposition. This results in a lower percentage of paramagnetic to diamagnetic grains and lowers the magnetic susceptibility of the rock. During a RST, the source of terrigenous grains is closer, resulting in a higher percentage of paramagnetic grains, and thus raises the magnetic susceptibility of the rock (Figure 6).

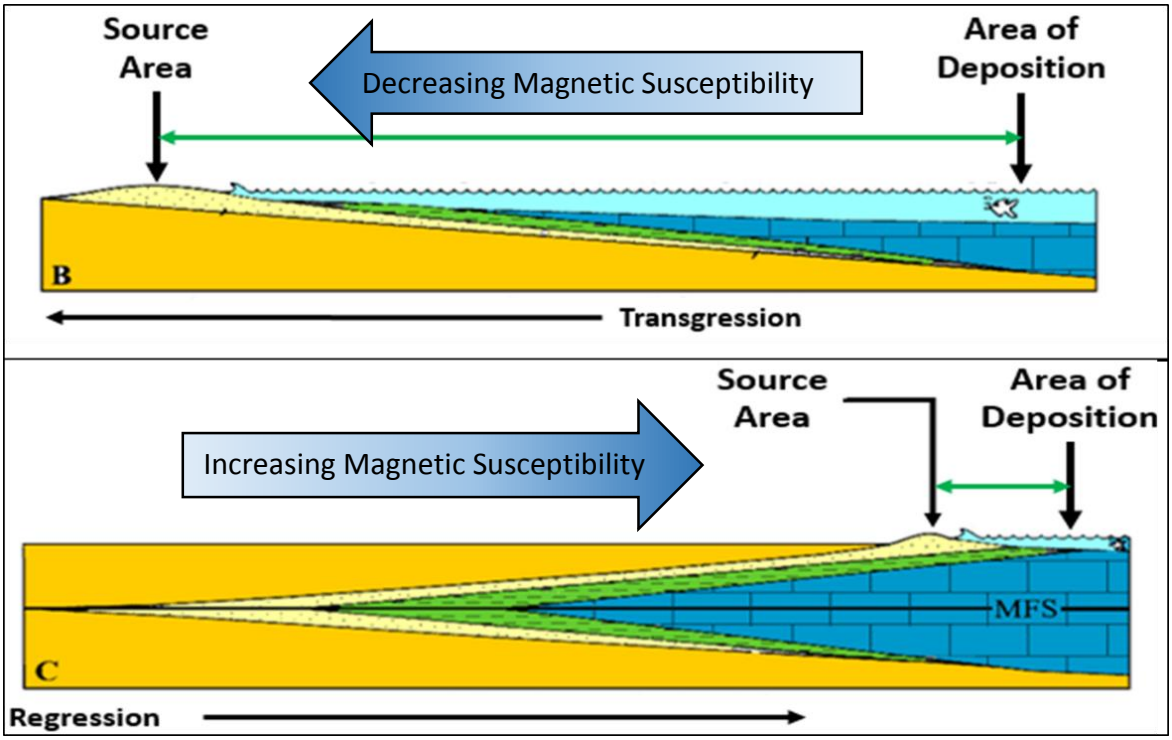

Figure 6. Transgression and regression controls the distance between source area and area of deposition. This distance controls the percentage of marine grains to terrestrial grains. Modified from Catuneanu (2002).

The relationship between magnetic susceptibility and T-R cycles has been demonstrated in the Devonian, Carboniferous, middle Permian, and Upper Cretaceous rocks in areas such as China (Zhang, 2000), Morocco and Bolivia (Ellwood, 2001), Alberta (Whalen and Day, 2008), Colorado (Ellwood, 2013a), and west Texas (Ellwood, 2013b). Specifically magnetic susceptibility has been used to correlate global changes in sea level by comparing measurements from well documented and biostratigraphically controlled Devonian outcrops in Morocco and Spain to cuttings from a Bolivian well (Ellwood, 2001)(Figure 7). The effectiveness of the technique has also been demonstrated on a biostratigraphically controlled section of Devonian carbonate in Alberta, Canada to a show details of events as small as the 4th order (Whalen & Day, 2008)(Figure 8). Based upon these results, it was expected magnetic susceptibility could be a viable method to determine T-R cycles in the Middle Devonian of the Appalachian basin. Magnetic susceptibility would be comparable to the traditional methods of using gamma and density logs and may be used to provide another line of evidence to help constrain depositional history.

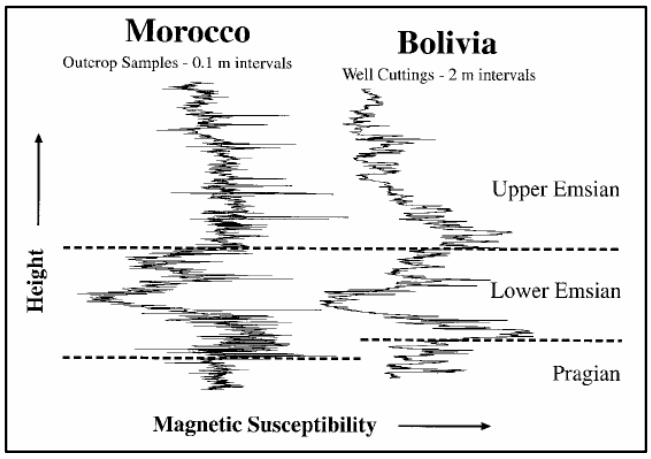

Figure 7. Magnetic susceptibility measurements on an outcrop in Morocco and well cuttings from Bolivia. The ages listed are biostratigraphically controlled from the Moroccan outcrop (Ellwood, 2001).

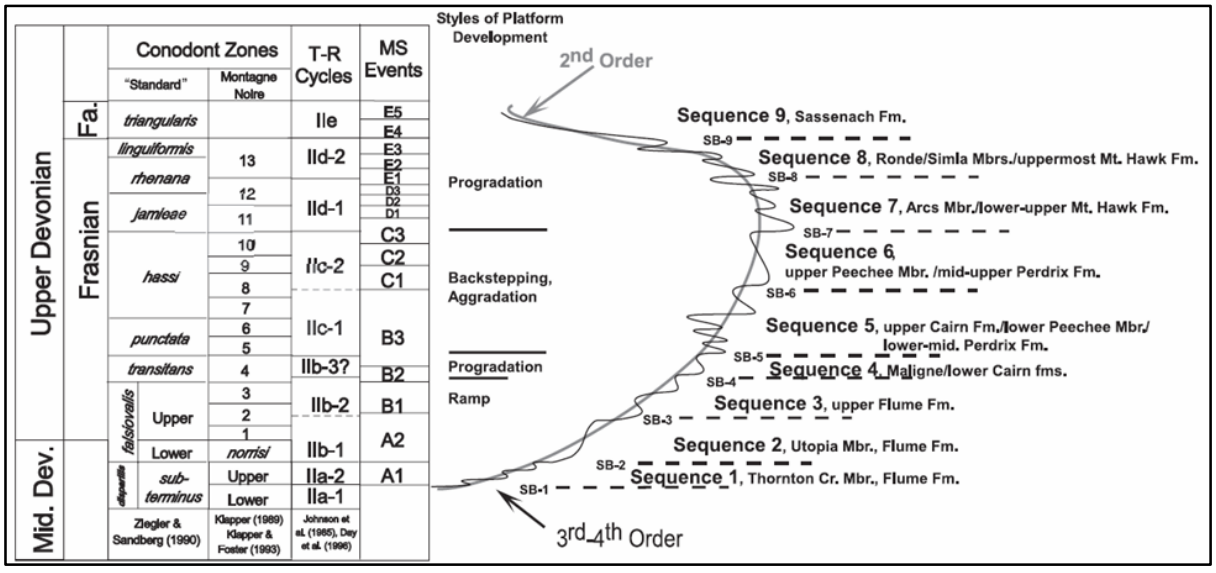

Figure 8. Biostratigraphically controlled Devonian carbonate in Alberta, Canada. Magnetic susceptibility events (peaks and troughs) were correlated with TST-RST cycles (T-R Cycles) as well as ages derived from conodonts (Whalen and Day, 2008).

It has been advanced that T-R cycles can be related to brittleness in gas bearing shale formations (Slatt, 2014)(Figure 9). It was expected that magnetic susceptibility could be correlated to the brittleness of the formation through these cycles. Specifically, in the siliciclastic dominated Marcellus Shale, high susceptibility values would correlate to a high brittleness and low susceptibility values would correlate to a low brittleness. The reasoning for this hypothesis is that, during a TST, the percentage of clays and organic carbon increase with respect to the more rigid terrigenous grains of quartz resulting in a more ductile rock as measured by a higher Poisson's ratio and lower Young's modulus. The inverse was also

expected, that during a RST, the percentage of quartz would increase while clays and organic carbon decrease and that this would produces a more brittle rock with a lower Poisson's ratio and higher Young's modulus. If however, it is a carbonate dominated play, a RST would increase the percentage of carbonates and produce a ductile rock. This correlation between magnetic susceptibility and siliciclastic content could be helpful for hydrocarbon exploration as brittle rocks are easier to fracture, tend to create a more extensive fracture network, and keep fractures open for longer periods of time. More ductile rocks tend to display opposing characteristics. They are more difficult to fracture and create a less extensive fracture network that is more easily closed. It was expected that, by studying the sequence stratigraphy, one would be better able to identify brittle and ductile couplets within the formation allowing the targeting of areas that will maximize fracture networks and increase hydrocarbon recovery.

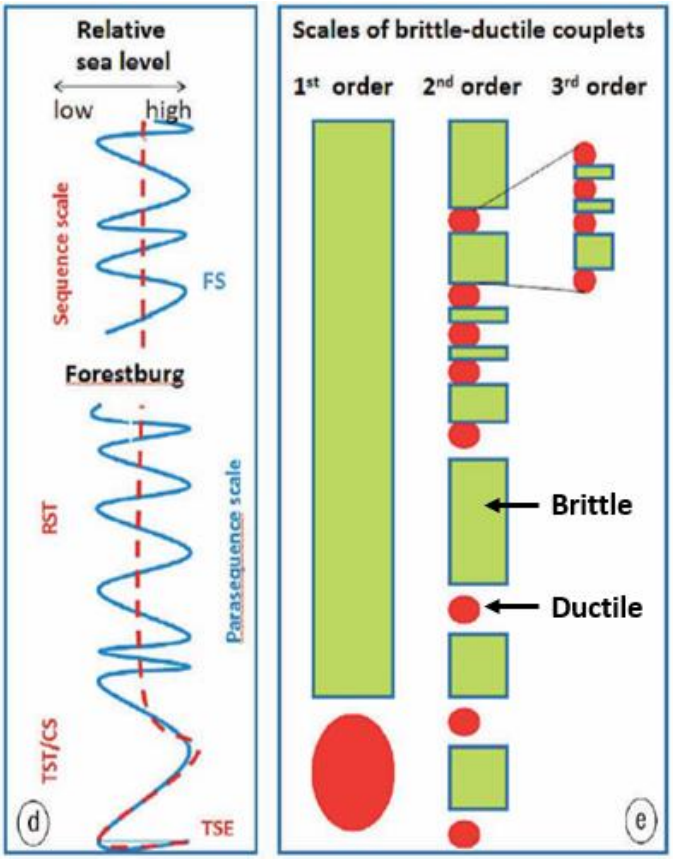

Figure 9. The 1st order sequence (red dashed line) shows the tendency toward a more ductile rock during TST and brittle rock during RST. This carries over to the parasequence scale (blue line). Modified from Slatt and Abousleimann (2011).

Dataset

The project centered on the Armstrong #1 well located in south-central Taylor County, West Virginia. This well was drilled in 2009 by the Petroleum Development Corporation (PDC). Several full log suites were provided by PDC along with 225.5 ‘of 4 “core, core description, and laboratory data containing vitrinite reflectance and total organic carbon content.

Methods

The project was conducted in four phases. The first phase was to determine the sequence stratigraphic framework of the well through conventional means. The second phase was to measure the magnetic susceptibility of the core in order to determine and compare a sequence stratigraphic framework independent from the conventional sequence stratigraphic. The third phase was to measure the brittleness of the formation using wireline logs and compare the results to the magnetic susceptibility and sequence stratigraphic frameworks to determine if a correlation exists. The final phase was to determine total organic carbon (TOC) content using common wireline techniques, compare the results to the susceptibility data, and correlate both to TOC samples taken directly from the core and measured by pyrolysis.

Magnetic Susceptibility

The core was measured with a Heritage Geophysics SM-30 magnetic susceptibility meter. The measurements were taken in intervals of 6 inches whenever possible (some sections of the core were missing). The raw susceptibility measurements are located in the Appendix. Susceptibility measurements were then loaded into IHS Petra™, a petrophysical analysis program to generate a magnetic susceptibility curve. Since the susceptibility meter measures volume susceptibility (κ), mass susceptibility (χ) was calculated as the final curve to be consistent with previous literature using the following equation (Nagata, 1961):

$$\chi = \frac{\kappa}{\rho},$$

where ρ is the bulk density curve and χ is expressed in m^3/kg. While mass susceptibility is helpful as a standard when comparing results to previous and subsequent work, volume susceptibility can be used if the analysis only compares relative changes such as sequence stratigraphy, and the measurements are made on an object of uniform volume. When volume susceptibility (κ) was compared to mass susceptibility (χ) on our uniform core, they were found to be practically identical with a correlation coefficient of 0.999 and standard error of 0.019 (Figure 10). Mass susceptibility values are most useful when comparing results from samples of differing volumes such as cuttings or if values are compared relative to mass such as values in weight percent.

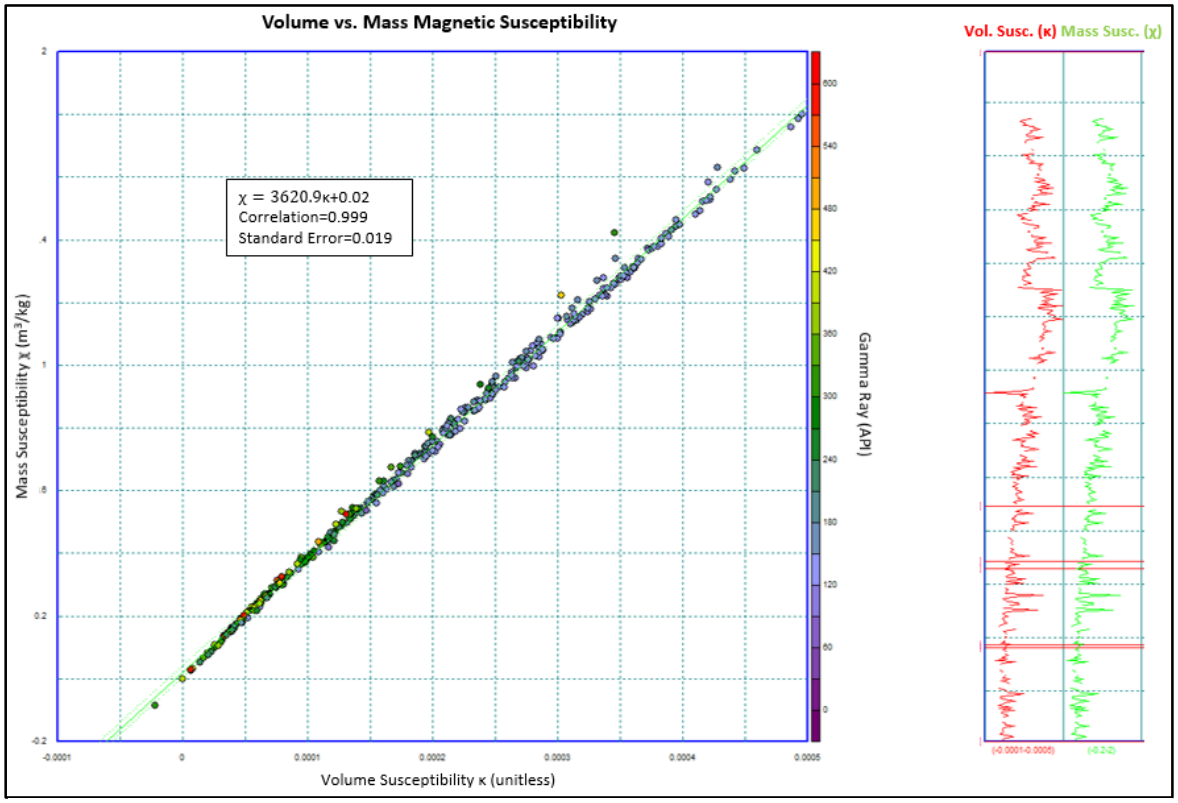

Figure 10. When mass and volume susceptibility are compared, they present a near exact correlation.

A variance test was also conducted to ensure the accuracy of the meter. Volume susceptibility was measured on a core taken from the Coldstream 1MH well in Clearfield County, Pennsylvania, drilled by the Energy Corporation of America. The tests were conducted at 3 locations on the core by taking 70 measurements each in the Marcellus shale at intervals of

~3 minutes between measurements. It was found that repeated exposure of the core to a magnetic field produced a series of increasing susceptibility values. The time interval between measurements was used to provide a rest period to prevent a remnant magnetization of the samples. The average variance between the three locations was 1.1×10^{-10} SI.

Raw mass susceptibility values were found useful in the Mahantango Formation, but were suppressed in the Marcellus Shale to such an extent that they were no longer useful (Figure 11). This was true for both volume and mass susceptibility measurements. It was determined that the suppression of the values was due to the kerogen content and that it would have to be factored out for the data to be useful. Since kerogen is a mixture dependent upon local conditions, its composition and susceptibility varies. Due to this, a value for kerogen was calculated by factoring out every other mineral in the matrix using:

$$\chi_{ker} = \frac{\chi_b - [(\chi_{Py} * W\%_{Py}) + (\chi_{Ill} * W\%_{Ill}) + (\chi_{Dol} * W\%_{Dol}) + (\chi_{Cal} * W\%_{Cal}) + (\chi_{Qz} * W\%_{Qz}) + (\chi_{Bar} * W\%_{Bar}) + (\chi_{Chl} * W\%_{Chl})]}{W\%_{Ker}},$$

where χ is mass susceptibility, W% is weight percent, Ker is kerogen, Py is pyrite, Ill is illite, Dol is dolomite, Cal is calcite, Qz is quartz, Bar is barite, Chl is chlorite, and χ_b is the mass susceptibility of the entire rock. With the exception of illite, mass susceptibility measurements were made using laboratory hand samples and dividing the results by the density of the mineral. The value for illite was taken from published data (Hunt, Banerjee, & Moskowitz, 1995). Once χ_{Ker} was calculated, it was then subtracted from χ_b to produce usable data (Figure 11). It was found that the χ_{Ker} value decreased logarithmically with depth. The best results were obtained by restricting the correction by depth and using only the mean χ_{Ker} in that interval using:

$$\chi_{Corr} = \chi_b - (\chi_{Avg} * W\%_{Ker}),$$

where χ_{Avg} is the mean mass susceptibility of kerogen for the interval. A summation of mean χ_{Ker} values is listed in Table 1.

Once the susceptibility of kerogen was removed, the data were in a usable state. The data still showed a decrease in value with depth, but also showed variation in the organic rich Marcellus Shale similar to the Mahantango Formation above. The upper, middle, and lower

Marcellus Shale units were also easily recognized. Variations in the data were then analyzed to determine T-R cycles. MFSs were chosen at susceptibility minimums and MRSs were chosen at susceptibility maximums. The resulting RSTs and TSTs fell between them. These T-R cycles were later compared to T-R cycles derived from the gamma ray and formation density logs.

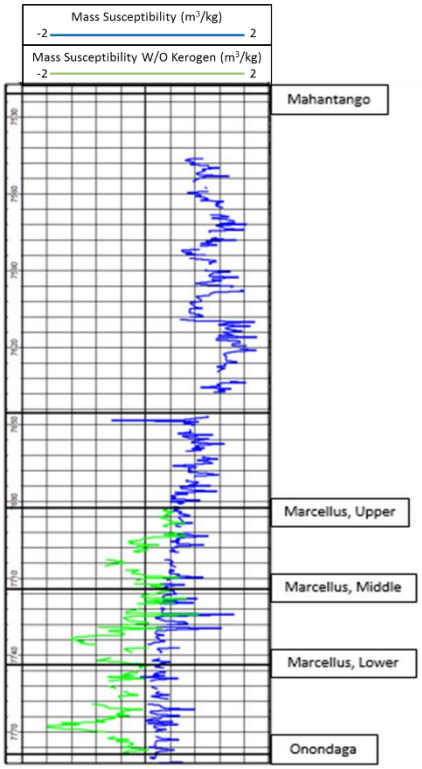

Figure 11. (Left) Variation in mass susceptibility is suppressed in the Marcellus shale due to kerogen content. When the kerogen content is removed, the variation is more readily observed.

Mean Susceptibility Values by Formation	
	Mean Susceptibility of Kerogen (χ_{avg})
Mahantango, upper	421.1 (m^3/kg)
Mahantango, lower	203.4 (m3/kg)
Marcellus, upper	24.0 (m3/kg)
Marcellus, middle	10.9 (m3/kg)
Marcellus, lower	4.8 (m3/kg)
Mahantango and Marecellus	118.0 (m3/kg)

Table 1. (Above) Mean χ_{Avg} values by formation. The values decrease logarithmically with depth. The lower Mahantango was designated based upon an increase in gamma and the presence of kerogen (Figure, 11).

Sequence Stratigraphy

The first goal of determining the sequence stratigraphic framework of the Marcellus shale was to establish the stratigraphic tops of the Mahantango Formation, Marcellus Shale, and Onondaga Limestone (Figure 12). This was accomplished using lithology, density and gamma ray logs. The top of the Mahantango was picked at 7520' based a decrease in gamma ray and drop in density corresponding to an increase in illite. Above this mark, the percent of calcite gradually rose indicating the Tully Limestone above. The top of the Marcellus was picked at 7646' based upon a sharp decrease in gamma ray and corresponding decreases in illite and kerogen. The Marcellus Shale was then subdivided into upper, middle, and lower members based upon lithology, gamma, and density. The tops of each of these subdivisions are indicated by a sharp decrease in gamma and increase in density. The top of the Onondaga

Limestone was picked at 7779' based upon a sharp drop in gamma and increase in calcite. The lithology for the Armstrong #1 was based upon Elan curve suites (Figure 12).

T-R cycles were then determined based upon wireline logs. The Middle Devonian shale formations of the Appalachian basin have been shown to encompass a 3rd order transgressive-regressive sequences and are part of a larger 2nd order sequence (Figure 3) (Lash & Engelder, 20011). These sequences are bound by maximum regressive surfaces (MRS) and maximum flooding surfaces (MFS) that are indicated by inverse changes in the gamma and density logs.

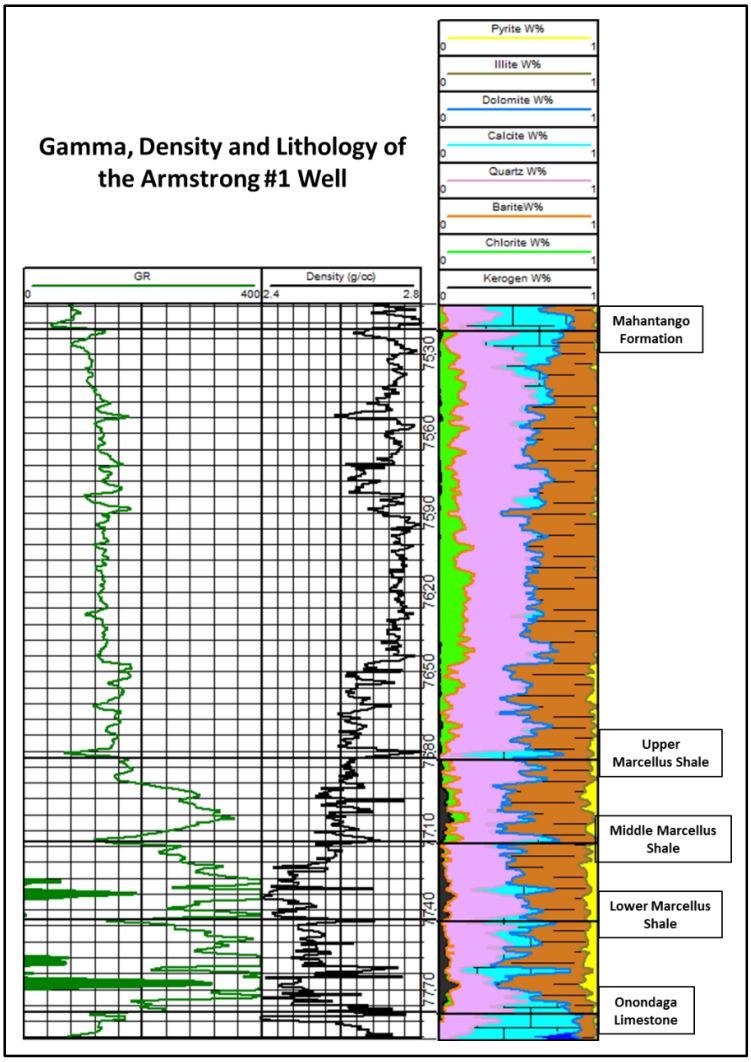

Figure 12. The placement of formation tops was based upon variations in gamma (Track 1), density (Track 2), and lithology (Track 3).

The MRS represents the lowest point of water depth, coincides with the formation tops, and the beginning of the transgressive systems tract (TST). This decrease in depth results in an increase of calcite and decrease of illite and is indicated by a corresponding decrease in gamma ray curve and increase in density. The MFS represents the highest point of water depth and the

beginning of the regressive systems tract (RST). This results in an increase of illite and corresponding increase in gamma-ray values and decrease in density.

Brittleness

The geomechanics of the formation were then classified based upon a brittleness index (BI) using both elastic properties and mineralogy. The brittleness index from mineralogy (BI_{min}) was calculated with the following equation (Wang & Gale, 2009):

$$BI_{min} = \frac{Qz+Dol}{Qz+Dol+Ca+Cly+TOC},$$

where Qz is quartz, Dol is dolomite, Ca is calcite, Cly is clay and TOC in total organic carbon.

The brittleness index based upon elastic properties (BI_{el}) used Poison's Ratio (E) and Young's Modulus (ν). These were calculated from the logs using the following equations:

Poisson's Ratio (E)

$$E = \frac{\left[0.5*\left(\frac{DT_S}{DT_C}\right)^2 - 1\right]}{\left[\left(\frac{DT_S}{DT_C}\right)^2 - 1\right]}, \text{ and}$$

Young's Modulus (ν)

$$N = \frac{13400\rho}{{DT_S}^2}$$

$$\nu = 2N(1+E),$$

where DT_S is the sonic shear log, DT_C is the sonic compression log, N is the shear modulus, and ρ is density. The brittleness index was determined from the following equations (Perez & Marfurt, 2013):

$$\nu_{Brit} = \frac{(\nu-\nu_{max})}{(\nu_{min}-\nu_{max})},$$

$$E_{Brit} = \frac{(E-E_{min})}{(E_{max}-E_{min})}, \text{ and}$$

$$BI_{el} = \frac{(\nu_{Brit}+E_{Brit})}{2},$$

where minimum and maximum values are obtained from cross-plotting E and v logs (Figure 13). The results from both methods were then plotted and classified into four categories ranging from ductile to brittle. They were then compared to magnetic susceptibility and both sequence stratigraphic frameworks to determine whether a relationship exists and if it does which framework is the better model.

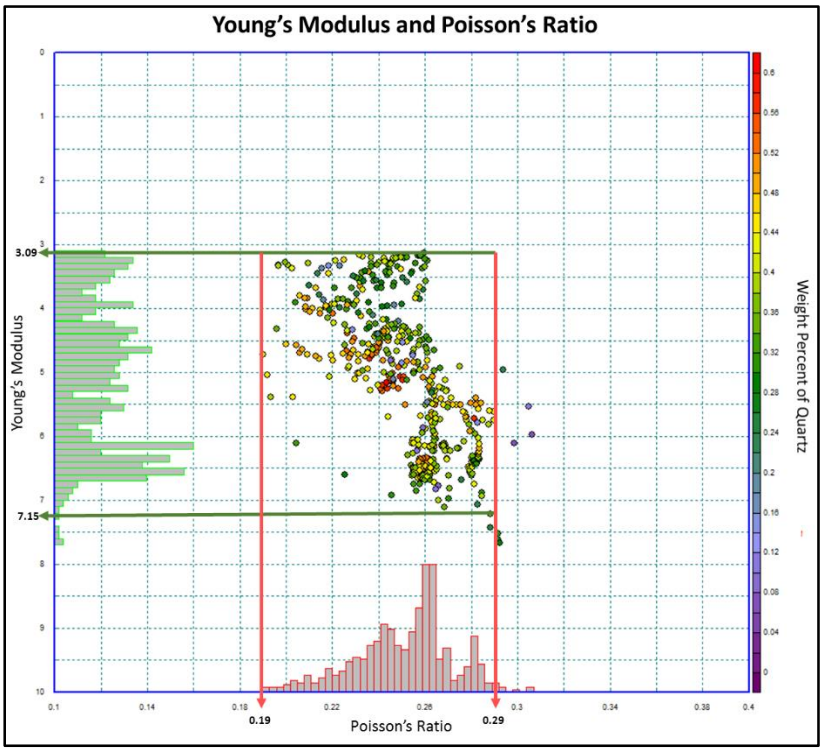

Figure 13. Minimum and maximum values for Poisson's Ratio and Young's Modulus. Note that high quartz areas correspond to low Poisson's Ratio values. The values used were: E_{max}=7.15, E_{min}=3.09, ν_{max}=0.29, and ν_{min}=0.19.

Organic Carbon

The well was analyzed based upon TOC. Three methods were used to calculate TOC. The first equation employs the density curve (Scmoker & Hester, 1983) as:

$$TOC = \left(\frac{154.497}{\rho}\right) - 57.261\ ,$$

where ρ is taken from the density log. This equation was developed for the Williston basin, but is popular in the Appalachian basin due to its simplicity and capacity to be calculated automatically in multiple wells (Scmoker & Hester, 1983). Schmoker's 1993 equation was also used.

$$TOC = 55.822\left[\left(\frac{\rho_b}{\rho}\right) - 1\right],$$

where ρ is taken from the density log and ρ_b is taken from an adjacent organic-poor interval. This equation was developed specifically for use in the Marcellus Shale and has proven useful. The effectiveness of both of Schmoker's equation diminishes in the eastern part of the basin, where the Armstrong #1 well is located (Schmoker, 1993). Because of this, these methods were supplemented by the Delta-logR technique (Passey Q. R., 1990). ΔlogR uses the sonic and resistivity logs as:

$$\Delta logR = \log_{10}\left(\frac{R}{R_{Baseline}}\right) - 0.02(\Delta t - \Delta t_{Baseline}),$$

where R is the resistivity curve, Δt is the sonic transit curve, and the baseline readings are taken from an adjacent organic poor interval. The difference, ΔlogR, is then fed into the corresponding TOC equation:

$$TOC = (\Delta logR) * 10^{(2.297 - 0.16888LOM)},$$

where LOM is the Level of Organic Metamorphism. This is typically a number from 6-12 and based upon vitrinite reflectance (R_o) values, but in the case of shale gas reservoirs where the LOM≥10.5 or Ro≥0.9, it is taken as a constant of 10.5 (Passey Q. R., 2010). Since the average vitrinite reflectance in the Armstrong #1 well is 1.40%, the constant of 10.5 was used. This equation has the advantage of calculating the effects TOC has on two different properties (sonic and resistivity), and factoring in maturity (LOM) to arrive at the answer using multiple lines of evidence. The results from these methods as well as the bulk magnetic susceptibility were compared to each other and the laboratory pyrolysis results provided with the Armstrong #1 well. Core TOC values were calculated using Rock-Eval pyrolysis by Weatherford Laboratories, and were used as the baseline to confirm the accuracy of other methods.

Results

Sequence Stratigraphy

When identifying T-R cycles using the traditional gamma-density method across both the Mahantango Formation and Marcellus Shale, a well-defined 2nd order cycle is evident with a MFS in the lower Marcellus shale and a continual regression through the Mahantango Formation. This same event is recognized using magnetic susceptibility (Figure 14). 3rd and 4th order cycles were found when the formations were analyzed on smaller scales. With the Marcellus shale recording three 3rd order T-R cycles. The MRS of these cycles corresponds to the tops of the upper, middle, and lower sections. Each of these 3rd order cycles was identified using both the traditional gamma-density method and magnetic susceptibility. In addition, two 4th order events are recorded in the lower and middle sections of the Marcellus Shale. Both small-scale events were identified as a drop in gamma ray and rise in density using the gamma-density technique. Only the 4th order cycle in the lower Marcellus Shale was identified using magnetic susceptibility (Figure 15). Three 3rd order T-R cycles, and two 4th order cycles are recognized in the Mahantango Formation. Each 3rd order T-R cycle in the Mahantango Formation was identified in both the gamma-density and magnetic susceptibility methods with very good correlation between the two. The first 4th order cycle was detected only with the gamma-density method and occurred at the boundary of the Marcellus Shale and Mahantango Formation. The second 4th order cycle occurred between 7598.0’ and 7609.5’ and was recorded only in the magnetic susceptibility log (Figure 16).

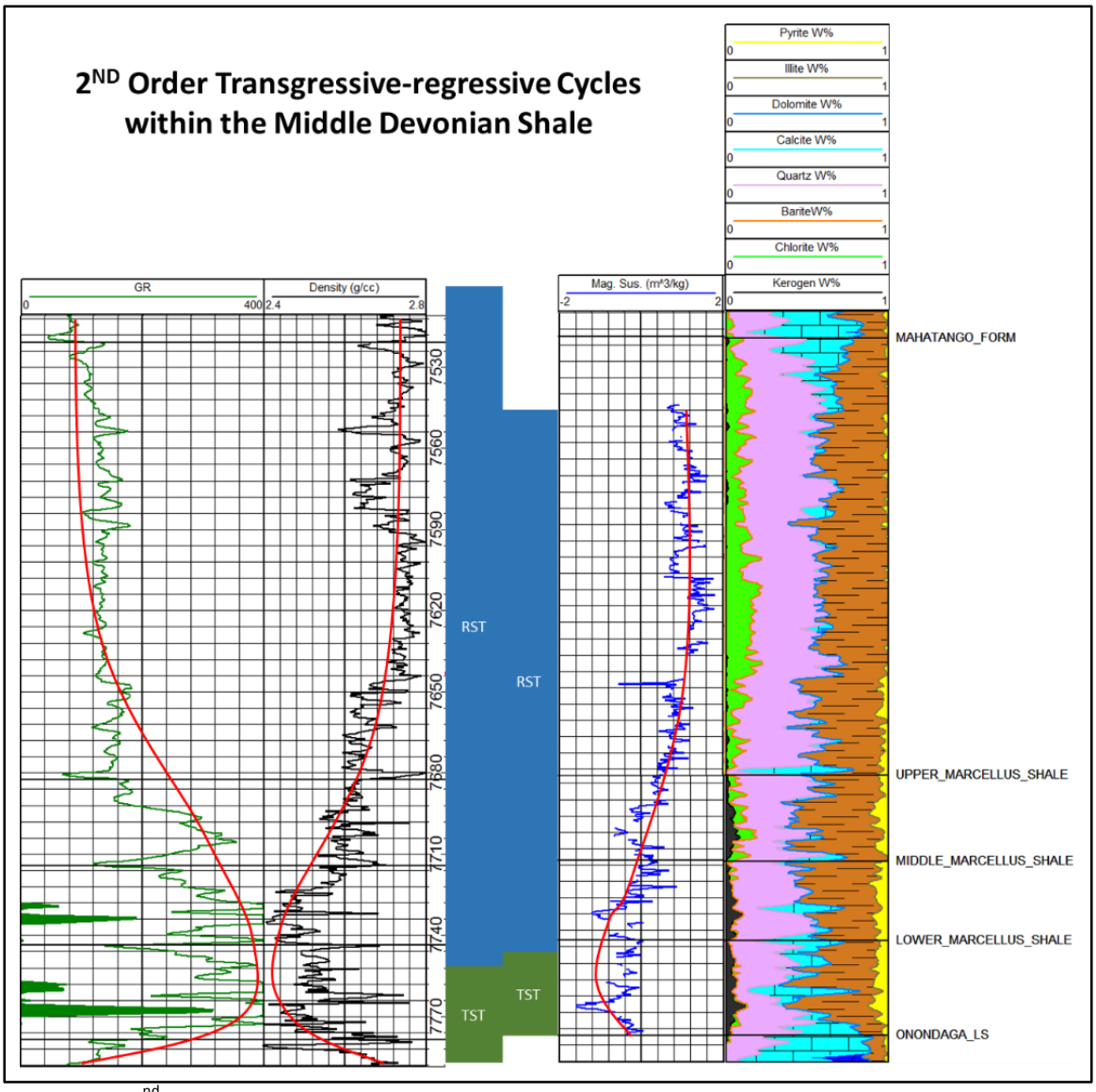

Figure 14. 2nd order transgressive-regressive cycle (red line) recorded in the Mahantango Formation and Marcellus Shale. **Track 1:** Gamma. **Track 2:** Density. **Track 3:** 2nd order TST-RST cycles based on the gamma-density method. **Track 4:** 2nd order TST-RST cycles based on magnetic susceptibility. **Track 5:** Mass susceptibility w/o kerogen. **Track 6:** ECS lithology curves.

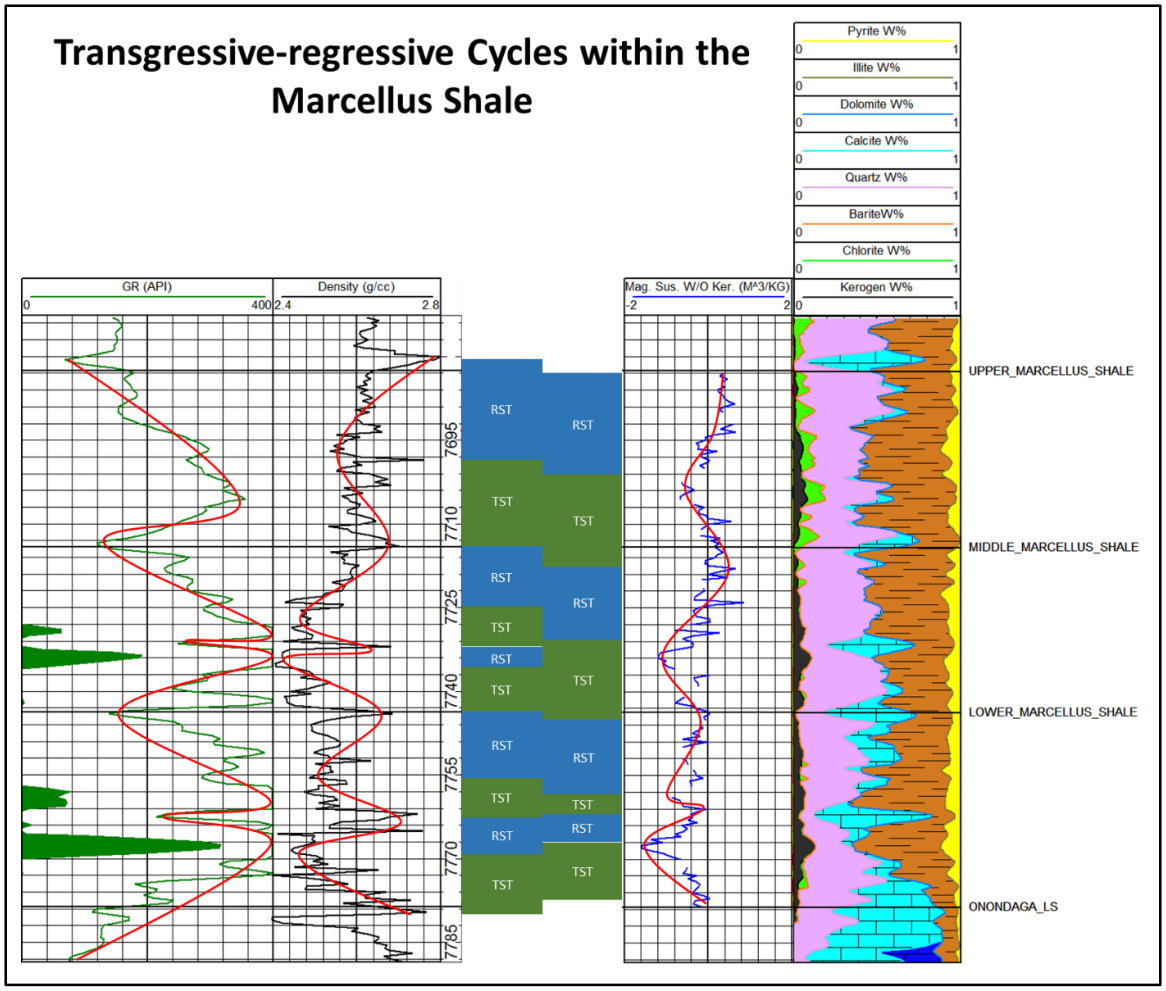

Figure 15. 3rd and 4th order cycles recorded in the Marcellus shale using both the gamma-density and magnetic susceptibility method. **Track 1:** Gamma, rugosity, and caliper. **Track 2:** Density. **Track 3:** 4th order T-R cycles based on the gamma-density method. **Track 4:** 4th order T-R cycles based on magnetic susceptibility. **Track 5:** Mass susceptibility w/o kerogen. **Track 6:** ECS lithology curves. The redline indicated the general trend of the data

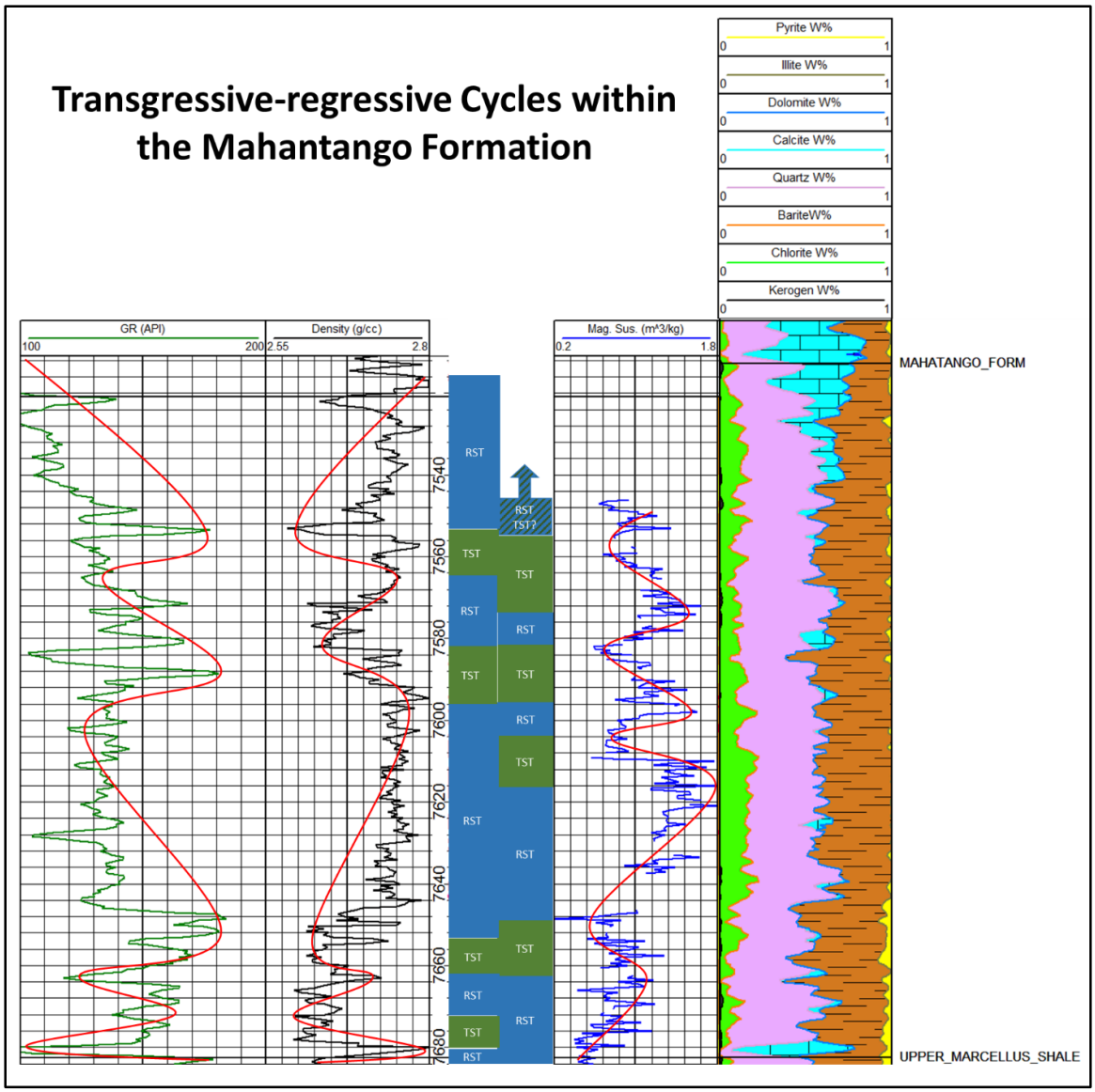

Figure 16. 3rd and 4th order cycles recorded in the Mahantango Formation using both the gamma-density and magnetic susceptibility method. **Track 1:** Gamma, rugosity, and caliper. **Track 2:** Density. **Track 3:** 4th order T-R cycles based on the gamma-density method. **Track 4:** 4th order T-R cycles based on magnetic susceptibility. **Track 5:** Mass susceptibility w/o kerogen. **Track 6:** ECS lithology curves. The red line indicates the general trend of the data.

Brittleness

The brittleness index (BI_{min}) is based upon mineralogy, and classified into four categories from ductile to brittle by plotting BI_{min} against density (figures 17, 18,19). This approach allowed for the best comparison of the variation of brittleness across the Mahantango Formation and Marcellus Shale (Figure 17). This approach was confirmed when plotting the Z-axis as core TOC, which shows the high TOC Marcellus Shale as more ductile and the low TOC Mahantango Formation as more brittle (Figure 18). The BI_{min} scale was then quartered across the range from 0-1 to show the relative brittle-ductile relationship (Figure 19). At first there appears to be no correlation between BI_{min} and the T-R cycles found earlier (Figure 20), but this only appears to be the case with the larger 2nd order cycle due to the exponential relationship of BI_{min} to density. Because BI_{min} drops considerably below the high gamma readings of the lower Mahantango at 7646', it was compared to each section separately and on the smaller scales of 3rd and 4th order cycles. It was first compared from the top of the Mahantango Formation to the top of the lower Mahantango Formation, then to the top of the lower Mahantango Formation to the bottom of the Marcellus Shale (figures 21, 22). When comparisons are made at this scale, better correlations exist and it can be seen that general trends in BI_{min} correspond to 3rd and 4th order TST-RST cycles. This is most evident in high gamma region from the lower Mahantango Formation and Marcellus Shale.

The brittleness index based upon elastic parameters (BI_{el}) was initially classified into the two categories of brittle and ductile based upon previous work (Figure 23) (Grieser & Bray, 2007). While this binary classification was empirically determined, it did not allow for a direct comparison to the relative classification of BI_{min} (Figure 24). To alleviate this, the results were quartered based upon their minimum and maximum values. This produced a relative range that included ductile, less ductile, less brittle, and brittle (Figure 25). It also allows for a direct comparison to BI_{min}. When compared to T-R cycles, BI_{el} showed little correlation at any scale (Figures 20, 26, and 27). Further, when compared directly to BI_{min}, there was no correlation between them (Figure 28). A direct comparison resulted in a 0.39 correlation coefficient with a standard error of 12.0 (Figure 29). In addition, no relationship between BI_{el} and magnetic susceptibility was observed.

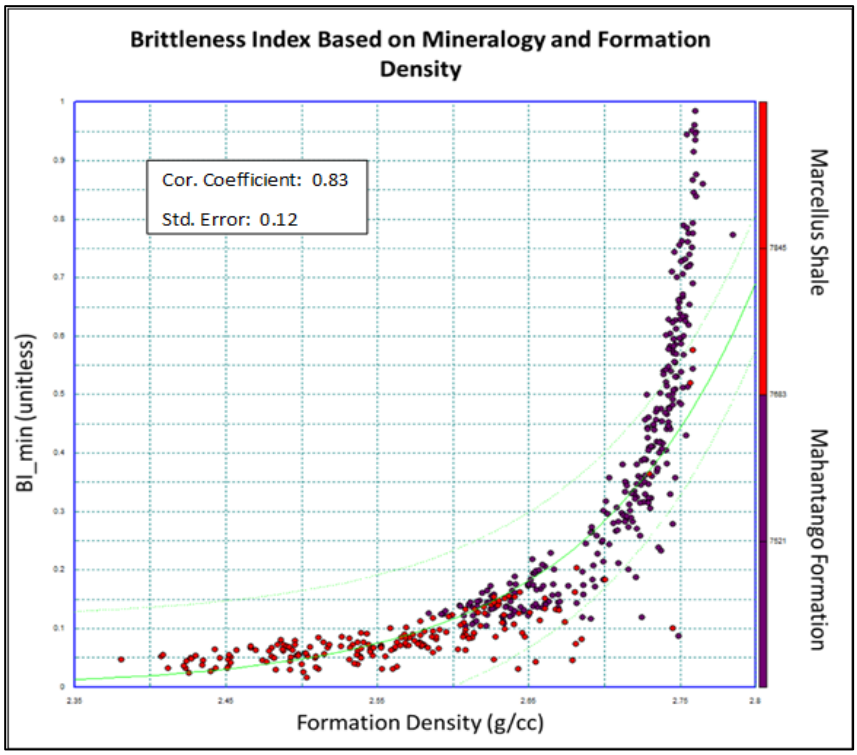

Figure 17. A comparison of BI_{min} and formation density shows an exponential relationship. The two shale units are easily distinguished.

Figure 18. A comparison of BI_{min} and formation density. Core derived TOC, plotted as the Z value, shows the high TOC Marcellus Shale as having a low BI_{min}.

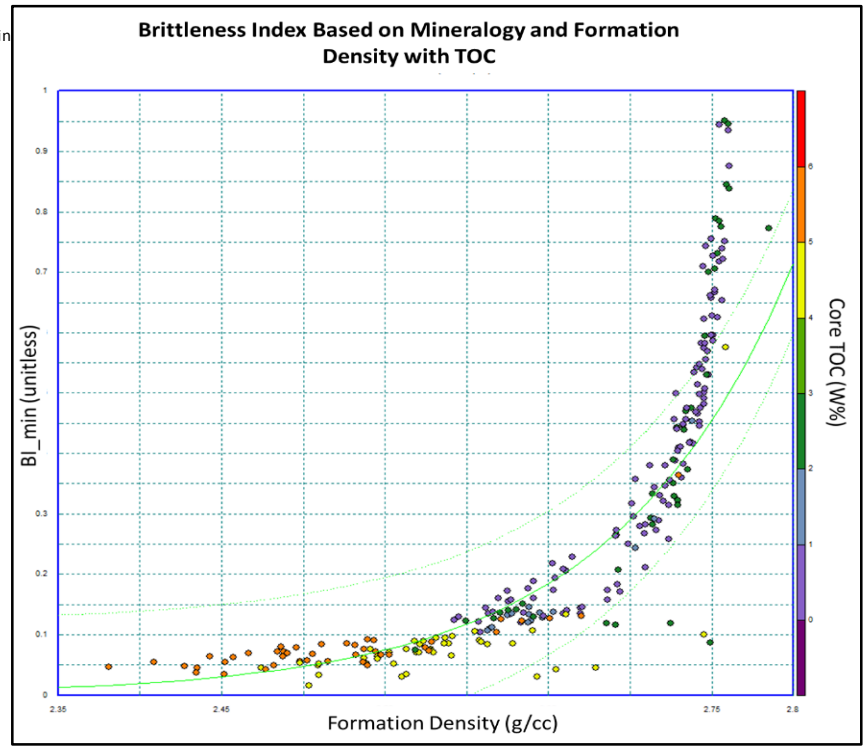

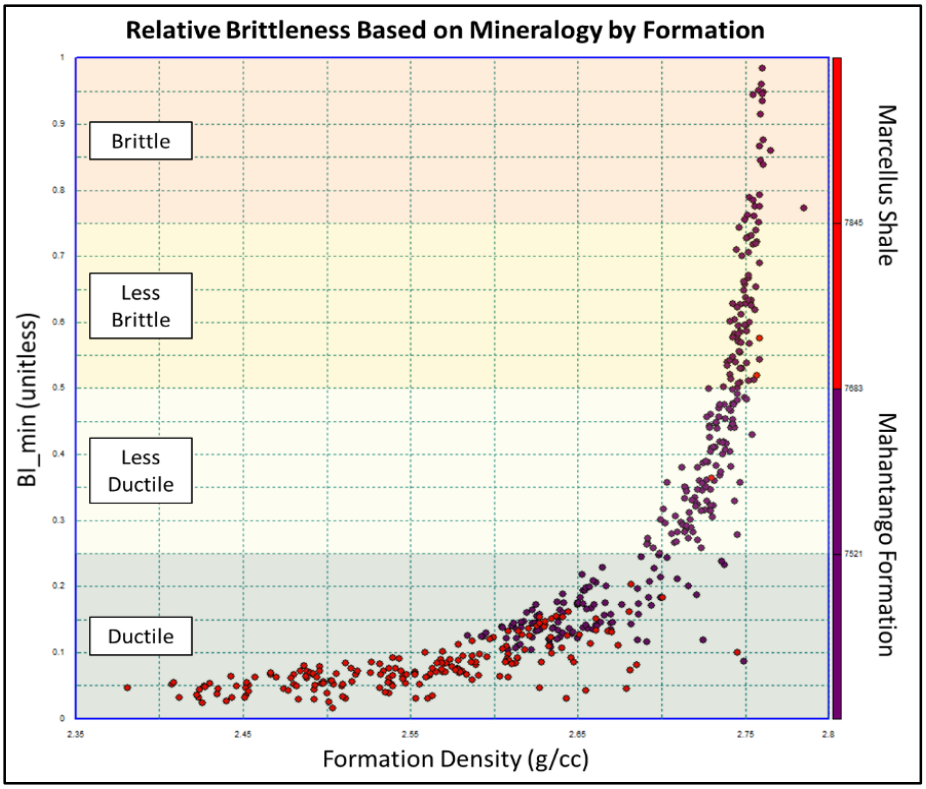

Figure 19. Relative brittleness of the Middle Devonian shale based upon mineralogy. **Ductile:** 0.0-0.25 Less **Ductile:** 0.25-0.50 Less **Brittle:** 0.50-0.75 Brittle**:** 0.75-1.0

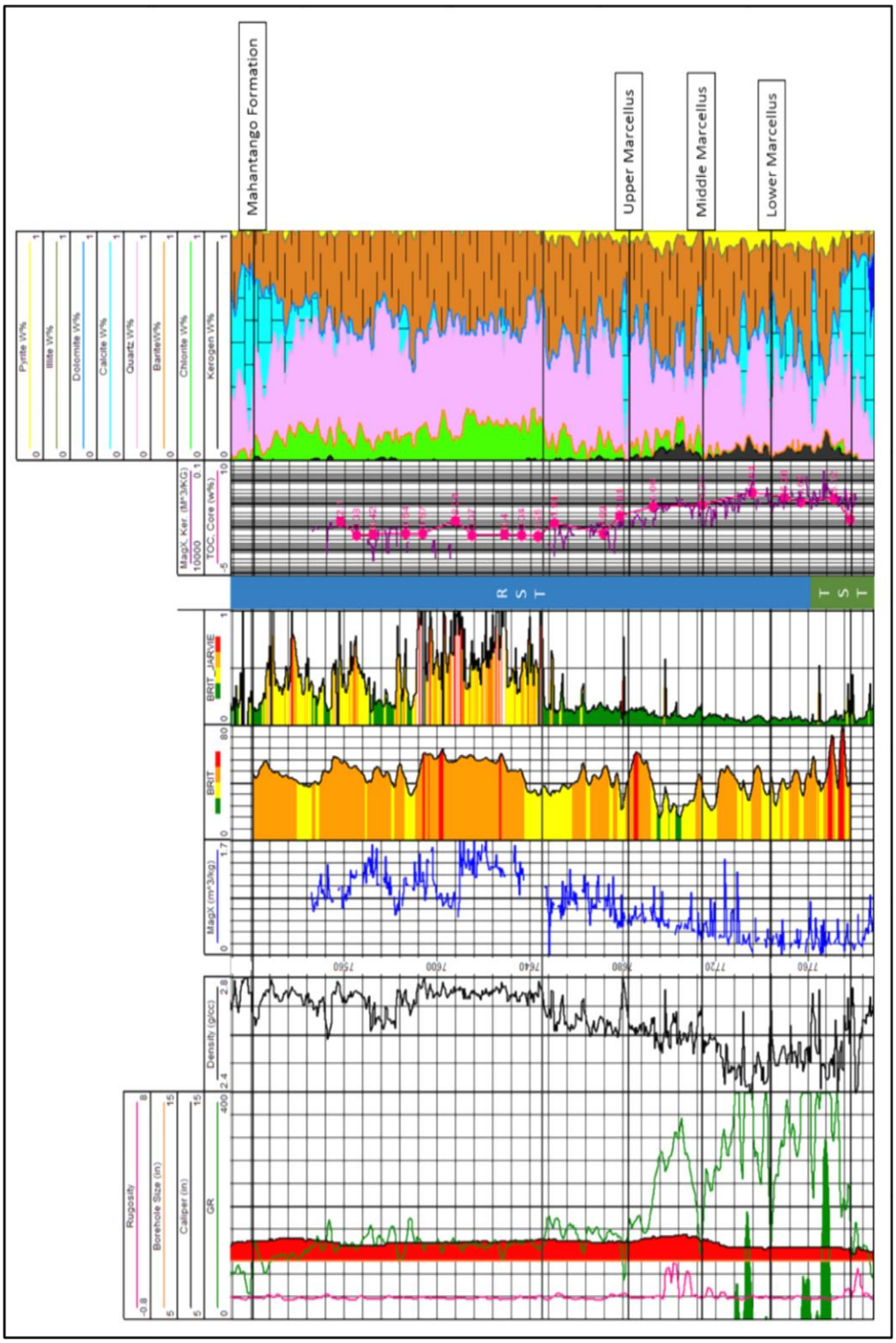

Figure 20. Wireline logs depicting: **Track 1.** Gamma, rugosity, and caliper. **Track 2.** Density. **Track 3.** Mass susceptibility. **Track 4.** BI_{el}. **Track 5.** BI_{min}. **Track 6.** 2nd order T-R. **Track 7.** Mass susceptibility of kerogen and core TOC. **Track 8.** ECS mineralogy logs.

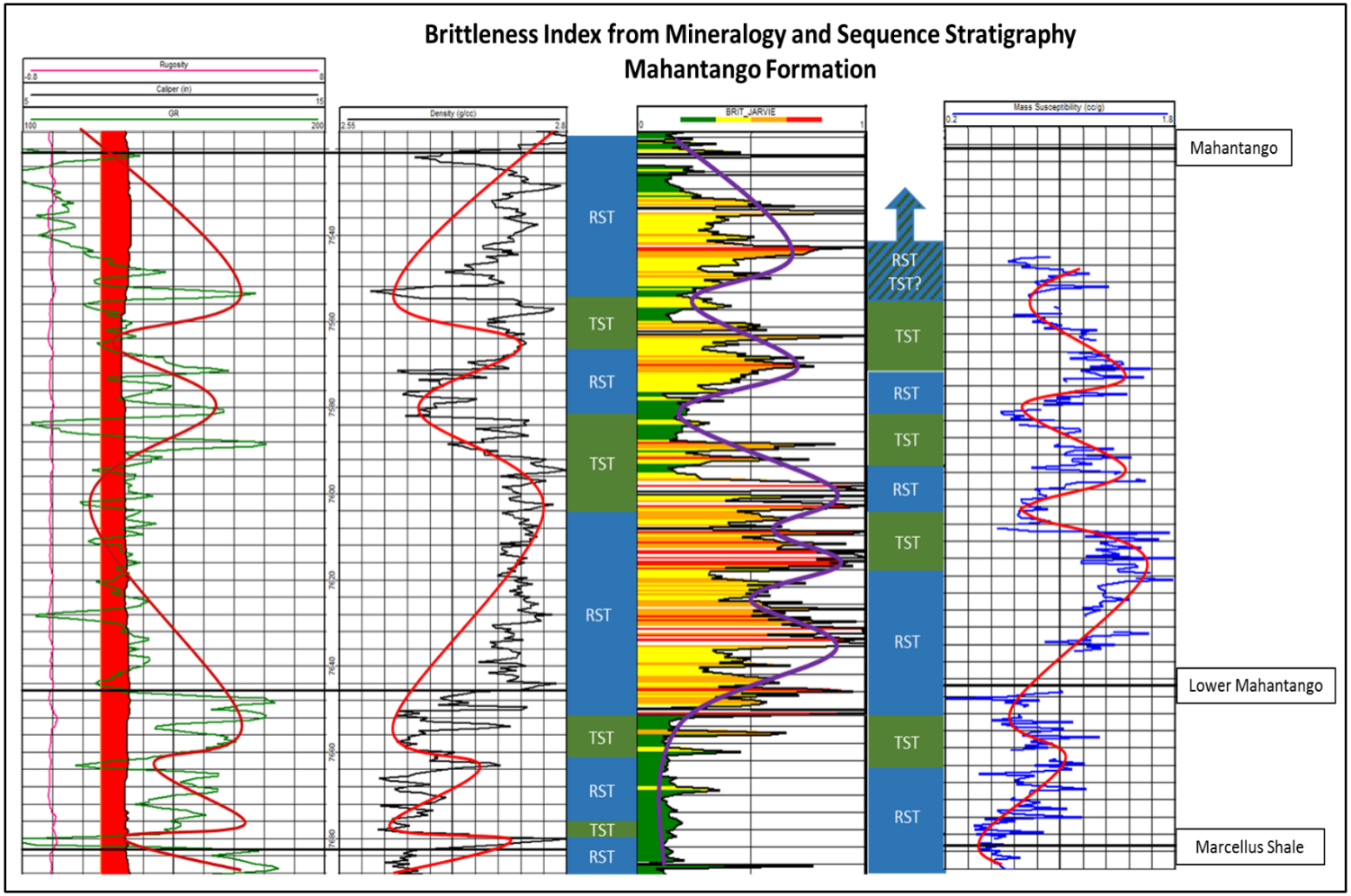

Figure 21. A comparison of trends in BI_{min} and 3rd-4th order TST-RST cycles. **Track1**. Gamma, rugosity, and caliper. **Track 2**. Density. **Track 3.** T-R from gamma/density. **Track 4.** BI_{min}. **Track 5.** T-R from magnetic susceptibility. **Track 6.** Magnetic susceptibility. Red and purple lines represent the general trend of the data.

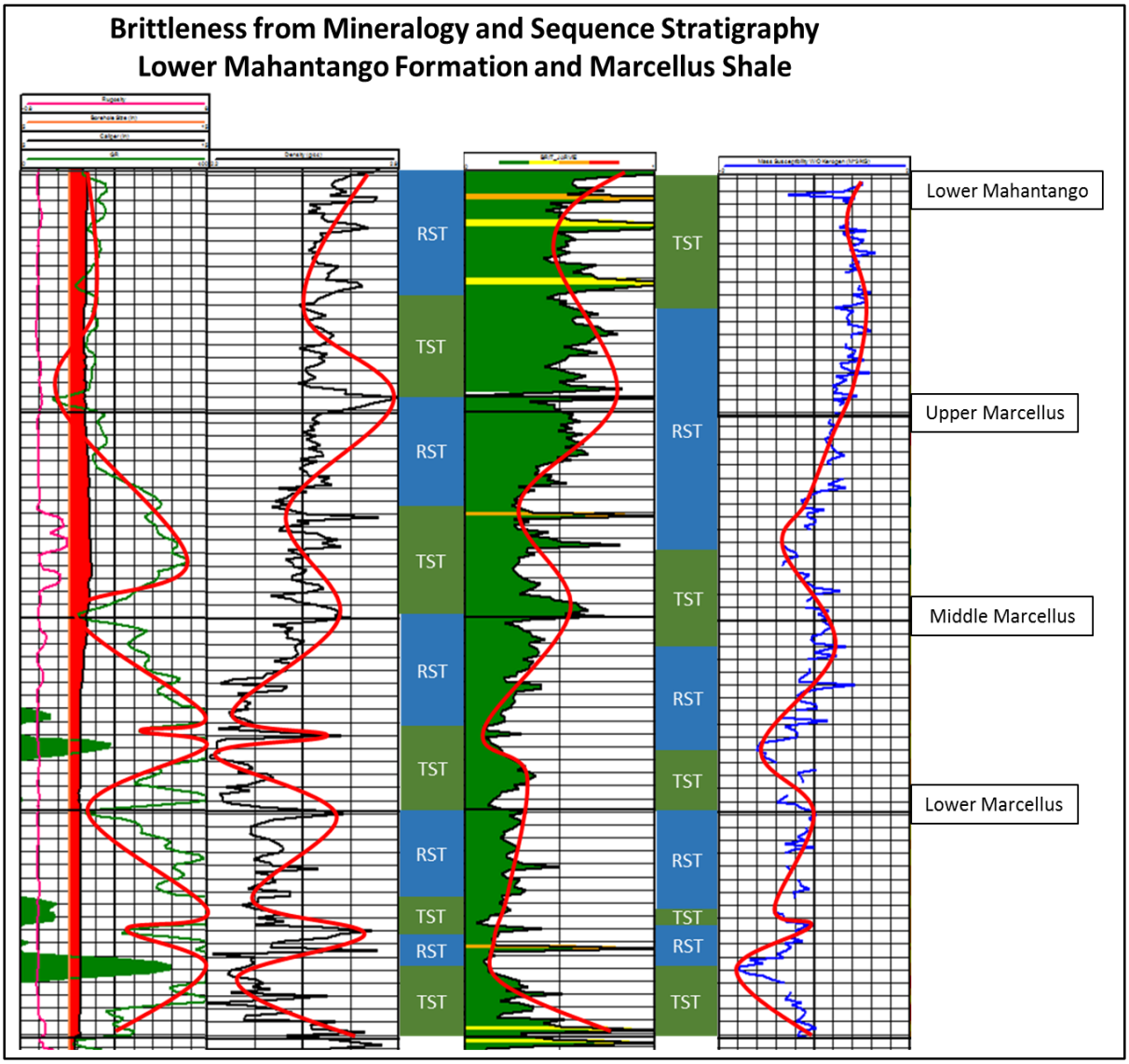

Figure 22. A comparison of trends in BI_{min} and 3rd-4th order T-R cycles. The red lines indicate the general trends of the data. Note that the scale of the BI_{min} has been reduced. **Track1**. Gamma, rugosity, and caliper. **Track 2**. Density. **Track 3.** T-R from gamma/density. **Track 4.** BI_{min}. **Track 5.** T-R from magnetic susceptibility. **Track 6.** Magnetic susceptibility.

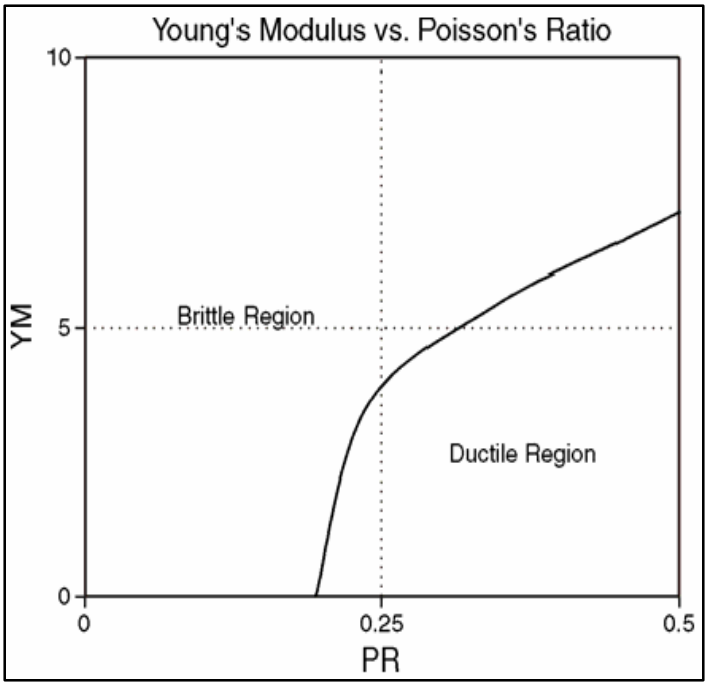

Figure 23. Initial template used to classify BI_{el} (Grieser & Bray, 2007). This binary classification did not compare well to the quaternary system used for BI_{min}.

Figure 24. A cross-plot of the elastic properties of Young's Modulus and Poisson's Ratio with the Mahantango Formation the Marcellus Shale as the Z axis.

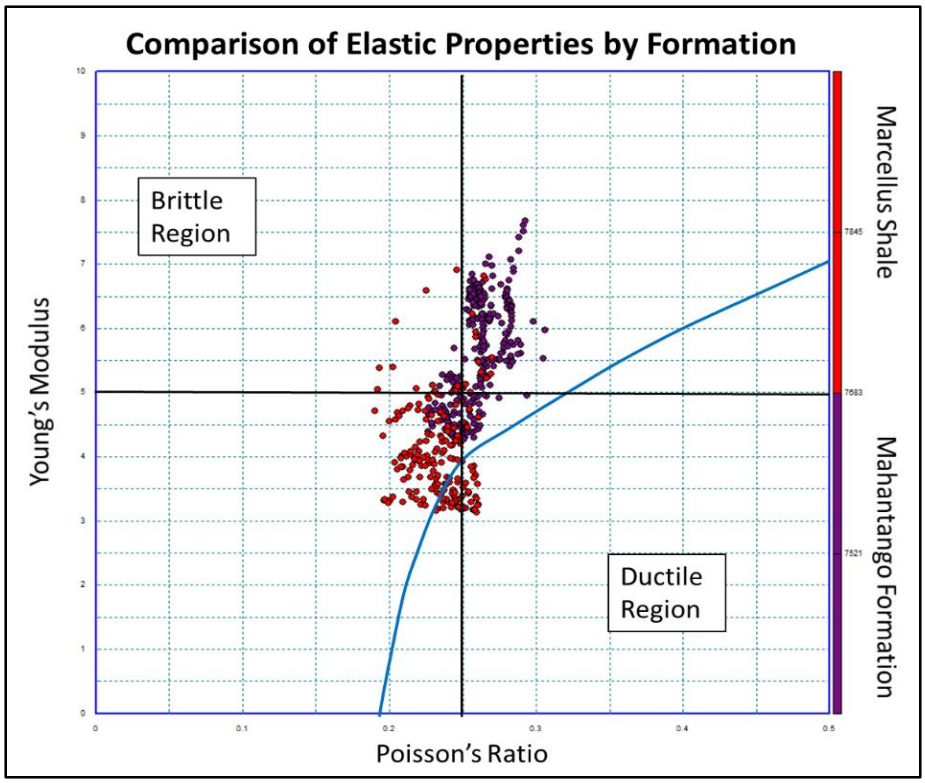

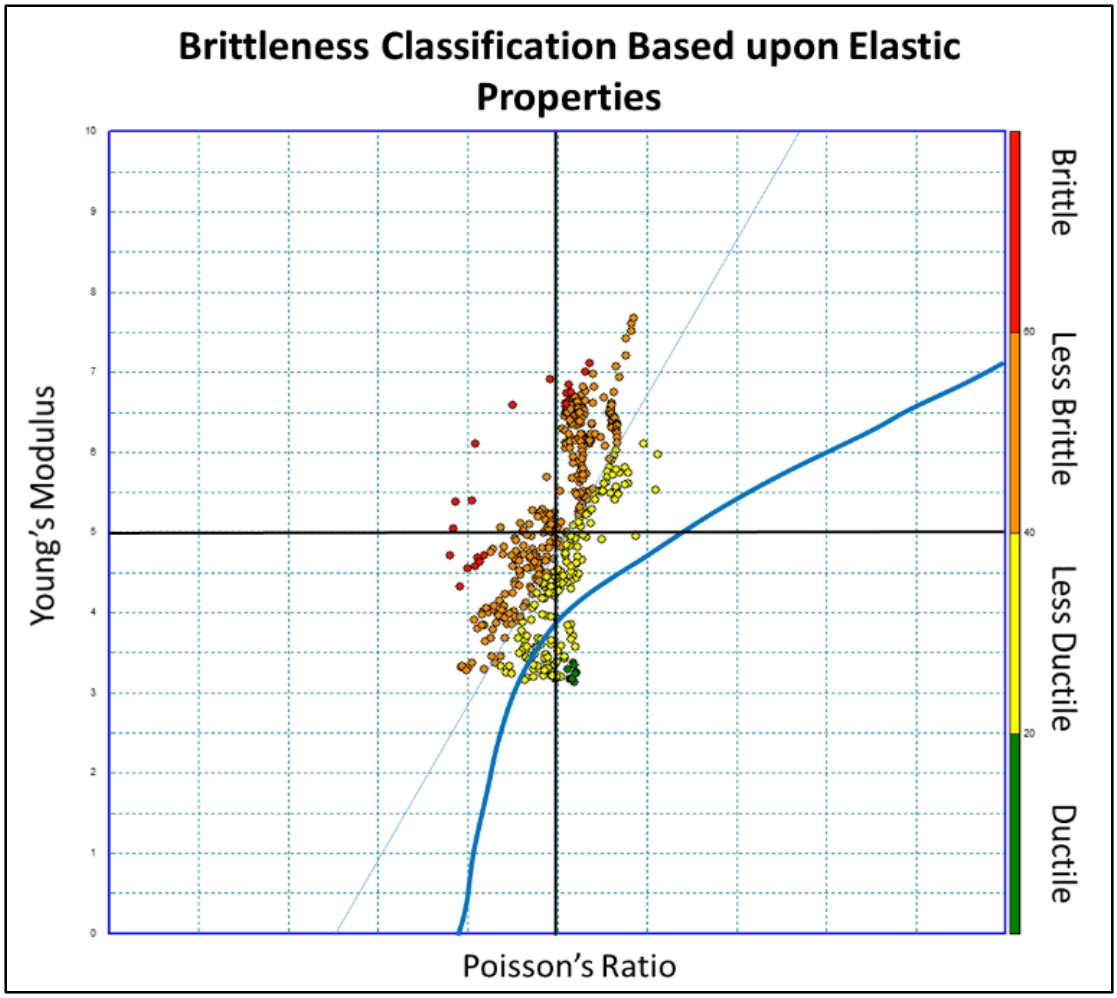

Figure 25. Relative brittleness classification system based upon elastic properties. Brittleness increases toward the upper left and decreases toward the lower right.

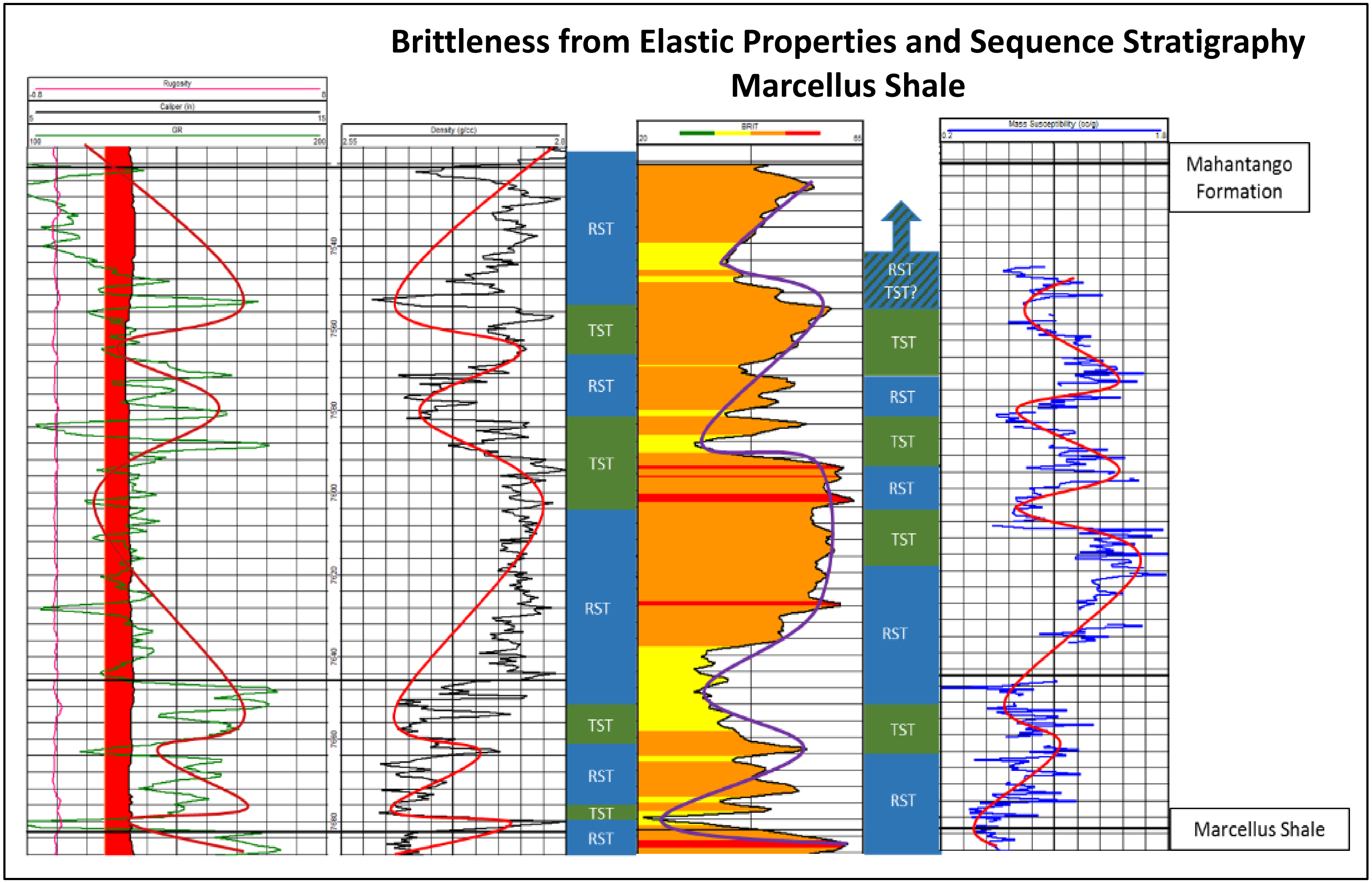

Figure 26. A comparison of trends in BI_{el} and 3^{rd}-4^{th} order T-R cycles. The red and purple lines indicate the general trends of the data. **Track1**. Gamma, rugosity, and caliper. **Track 2**. Density. **Track 3.** T-R from gamma/density. **Track 4.** BI_{el}. **Track 5.** T-R from magnetic susceptibility. **Track 6.** Magnetic susceptibility.

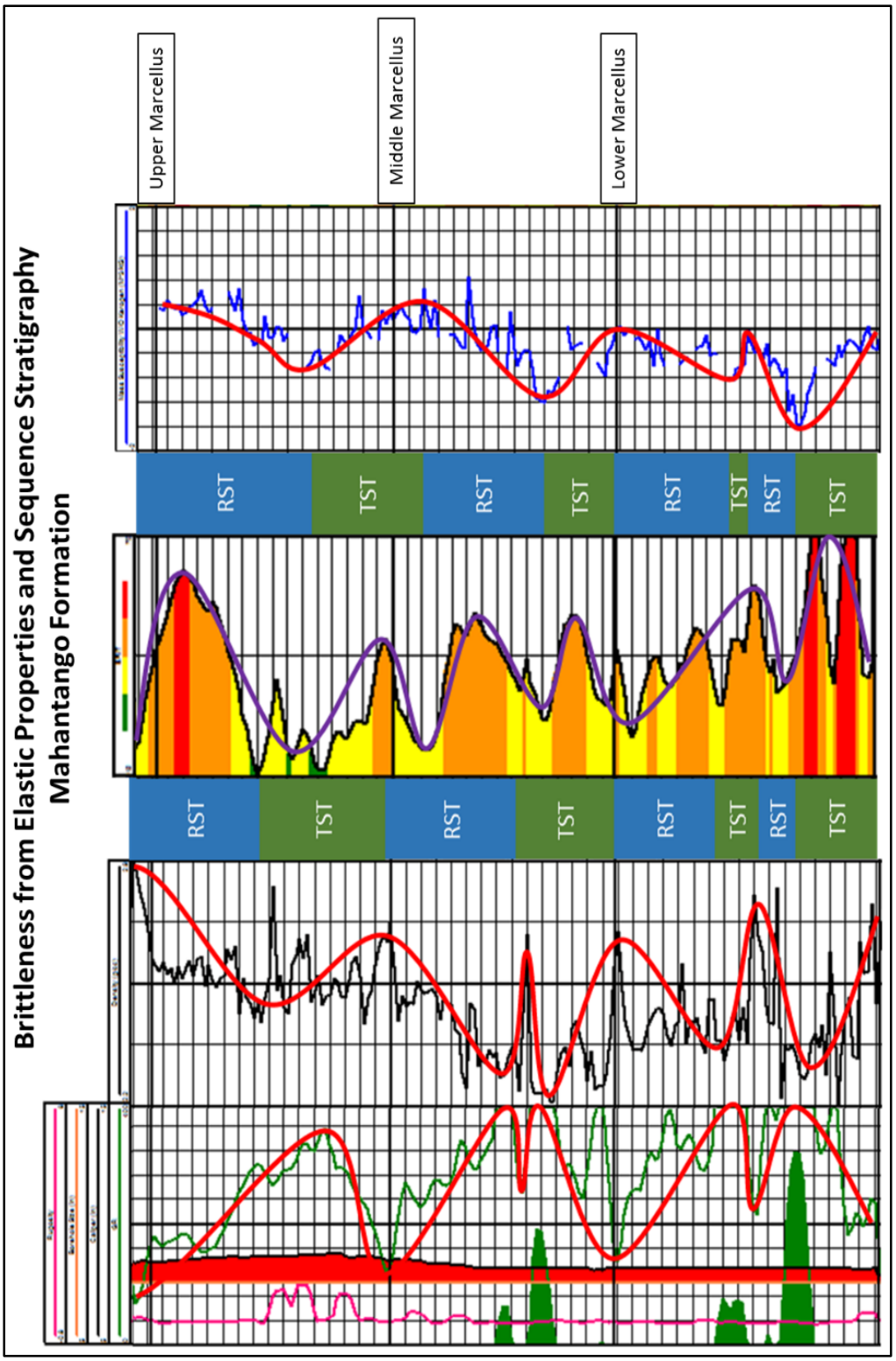

Figure 27. A comparison of trends in BI_{el} and 3rd-4th order TST-RST cycles. The red and purple lines indicate the general trends of the data. **Track 1**. Gamma, rugosity, and caliper. **Track 2**. Density. **Track 3.** T-R from gamma/density. **Track 4.** BI_{el}. **Track 5.** T-R from magnetic susceptibility. **Track 6.** Magnetic susceptibility.

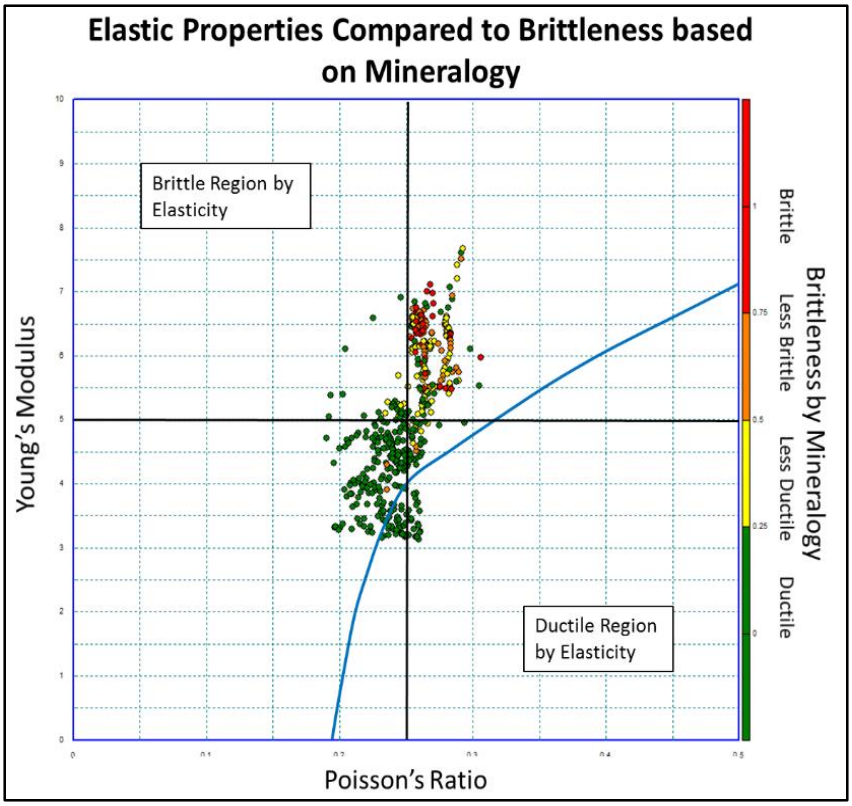

Figure 28. A comparison of BI_{el} and BI_{min} show no relationship between them. BI_{min} is shown as the z-axis.

Figure 29. No relationship was found between the brittleness index derived from elasticity or mineralogy.

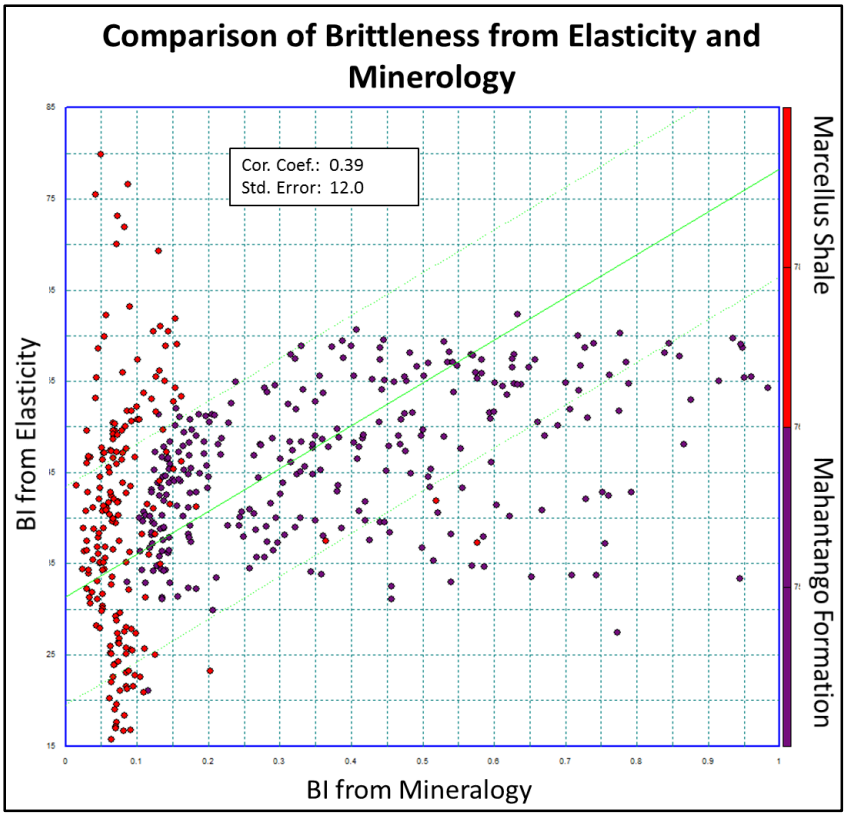

Organic Carbon

Of the three methods used to determine total organic carbon (TOC), Schmoker's 1993 equation was the most accurate, followed by his 1983 equation, and the ΔlogR method when both the Mahantango Formation and the Marcellus Shale were analyzed together (Table 2). When compared to the TOC values derived from the core, Schmoker's 1993 equation follows very closely to the logs and has a correlation coefficient of 0.78 with a margin of error of 1.36 (Figure 30). Schmoker's 1983 equation followed the same trend but only achieved a correlation coefficient of 0.74 with a margin of error of 1.46 (Figure 31). The ΔlogR method had the worst outcome with a correlation coefficient 0.73 and margin of error of 1.48 (Figure 32). When the magnetic susceptibility was compared to the core TOC values, they produced an inverse correlation with the mass susceptibility of the whole rock achieving a 0.79 correlation coefficient and margin of error of 1.25. Also, the 4th order cycle between 7598.0' and 7609.5' detected by an abrupt drop in susceptibility coincides with a spike in core TOC values (Figure 33). After the susceptibility of kerogen was removed, the adjusted susceptibility was compared to the core TOC values and found to have an inverse logarithmic relationship producing the highest correlation coefficient of 0.90 and lowest margin of error of 0.92 (Figure 34).

Comparion of Wireline Values to Rock-Eval TOC Estimates (Mahantango Formation and Marcellus Shale)		
	Corelation Coefficient	**Standard Error**
Schmoker (93)	0.78	1.36
Schmoker (83)	0.74	1.46
ΔlogR	0.73	1.48
Magnetic Susceptibility (χ_b)	0.79	1.25
Magnetic Susceptibility (χ_{Ker})	0.90	0.92

Table 2. Comparison of analytical methods of deriving TOC from wireline logs and core TOC values. Additional comparisons are made of the mass susceptibility of the whole core (X_b) and the mass susceptibility of kerogen (X_{ker}) to core TOC. Accuracy is shown based upon correlation coefficient and standard error.

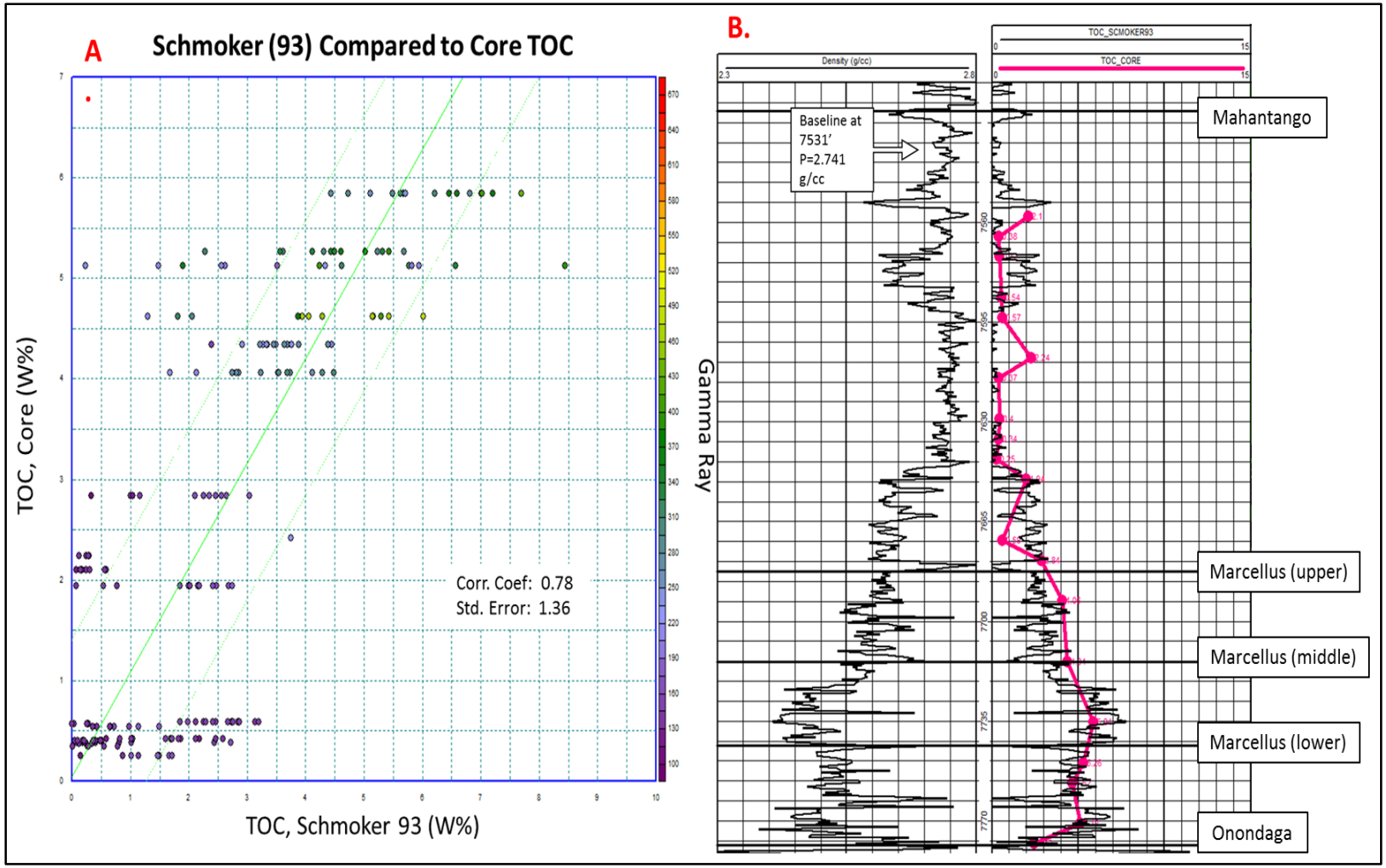

Figure 30. A. Comparison of TOC derived from Schmoker's 1993 equation and TOC derived from the core using Rock-Eval pyrolysis across both formations. The Z-axis is gamma ray. **B.** Wireline logs of density on the left and a combination of TOC from Schmoker 93 (black) and core TOC (pink) on the right.

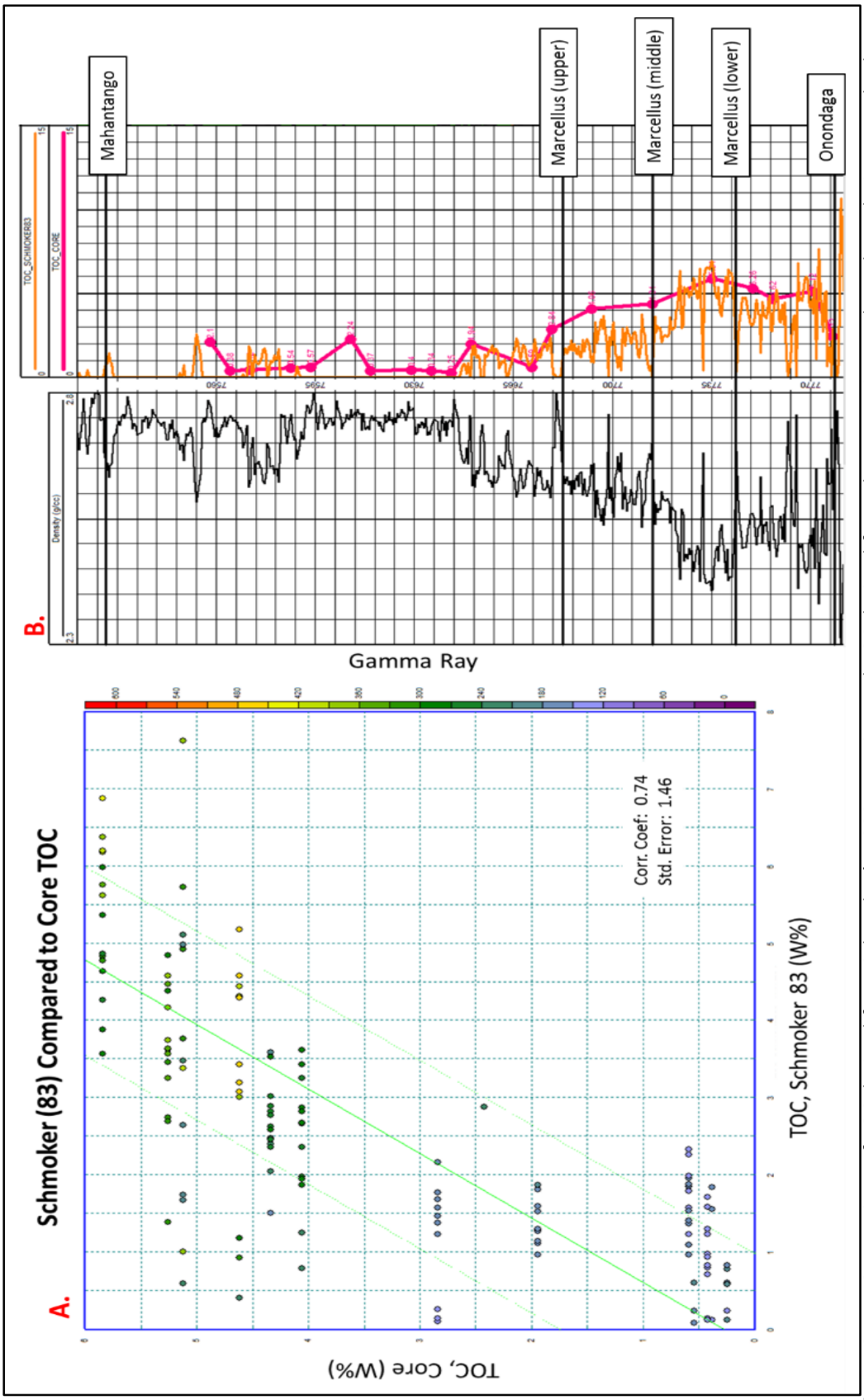

Figure 31. A. Comparison of TOC derived from Schmoker's 1983 equation and TOC derived from the core using Rock-Eval pyrolysis across both formations. The Z-axis is gamma ray. **B.** Wireline logs of density on the left and a combination of TOC from Schmoker 83 (orange) and core TOC (pink) on the right.

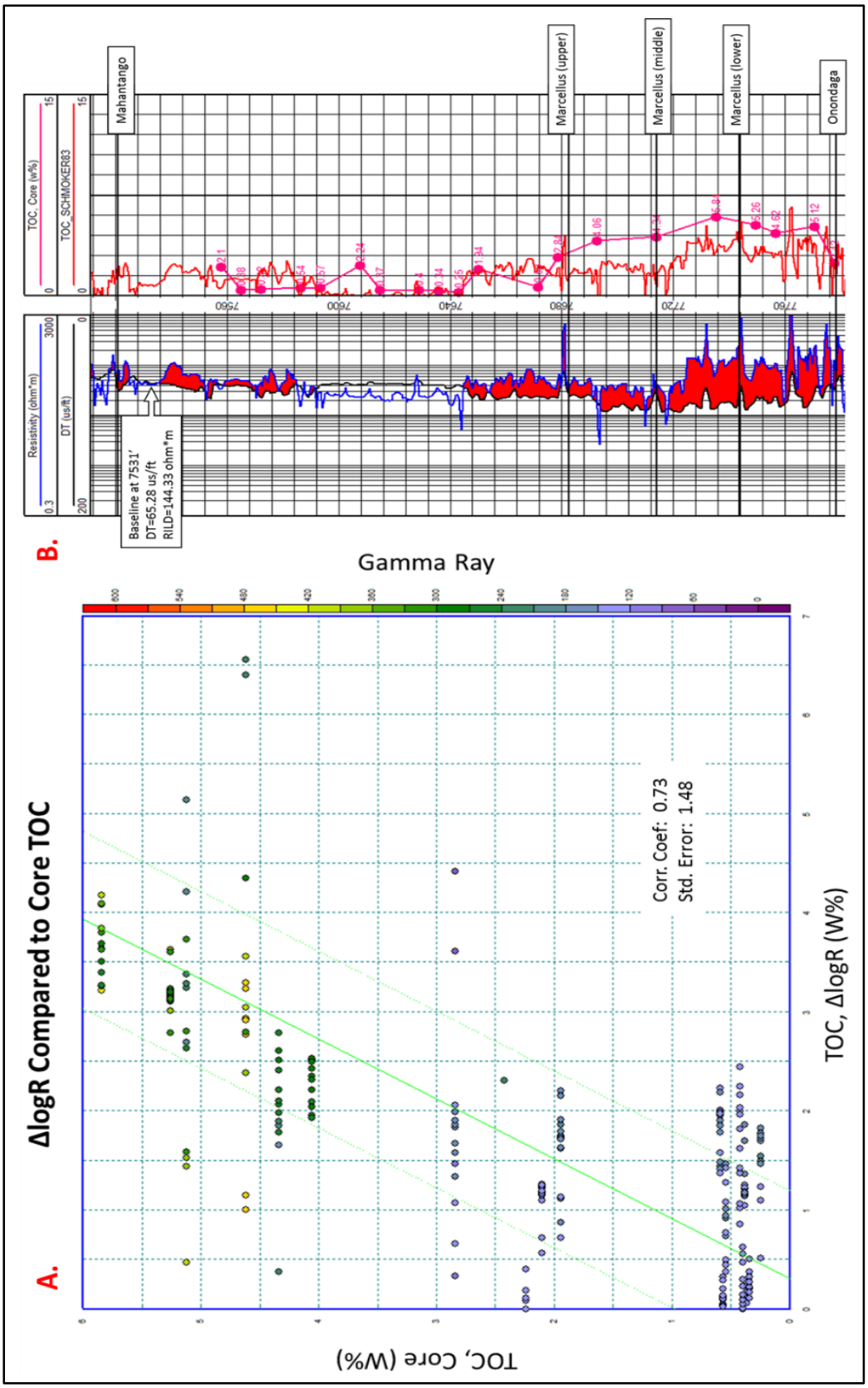

Figure 32. A. Comparison of TOC derived from the ΔlogR method and TOC derived from the core using Rock-Eval pyrolysis across both formations. The z-axis is gamma ray. **B.** Wireline logs of a combination of TOC from ΔlogR (orange) and core TOC (pink) on the right and a combination of resistivity (blue) and sonic (black) on the left. The red shaded area on the left is the overlap of sonic and resistivity indicating the presence of organic carbon.

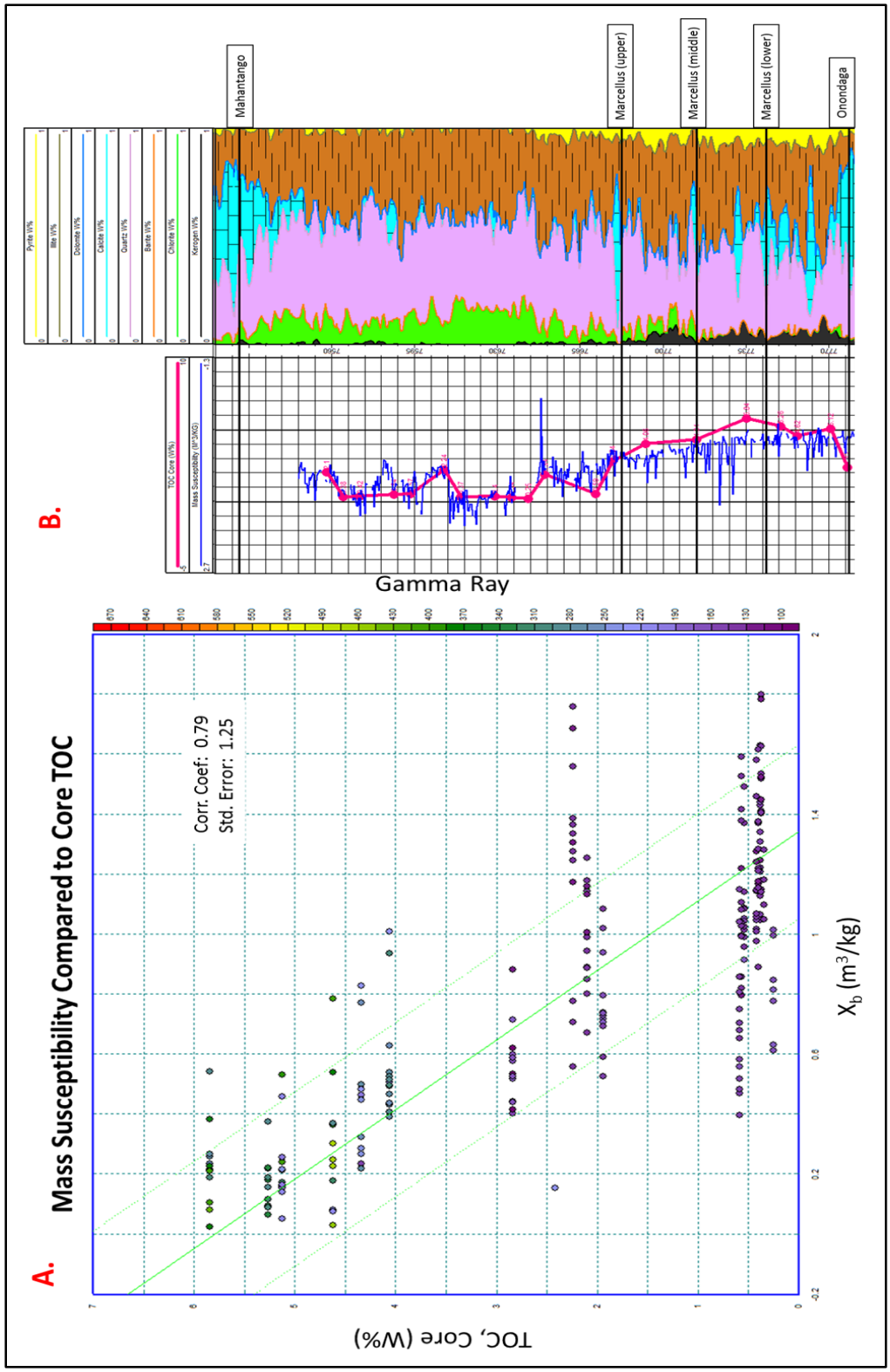

Figure 33. A. Comparison of mass susceptibility and TOC derived from the core using Rock-Eval pyrolysis across both formations. The z-axis is gamma ray. **B.** A combination of mass susceptibility (blue) and core TOC (pink) on the left and ECS mineralogy curves on the right. Note the mass susceptibility curve has been reversed and the increase in TOC at the 4th order cycle between 7598.0' and 7609.5'.

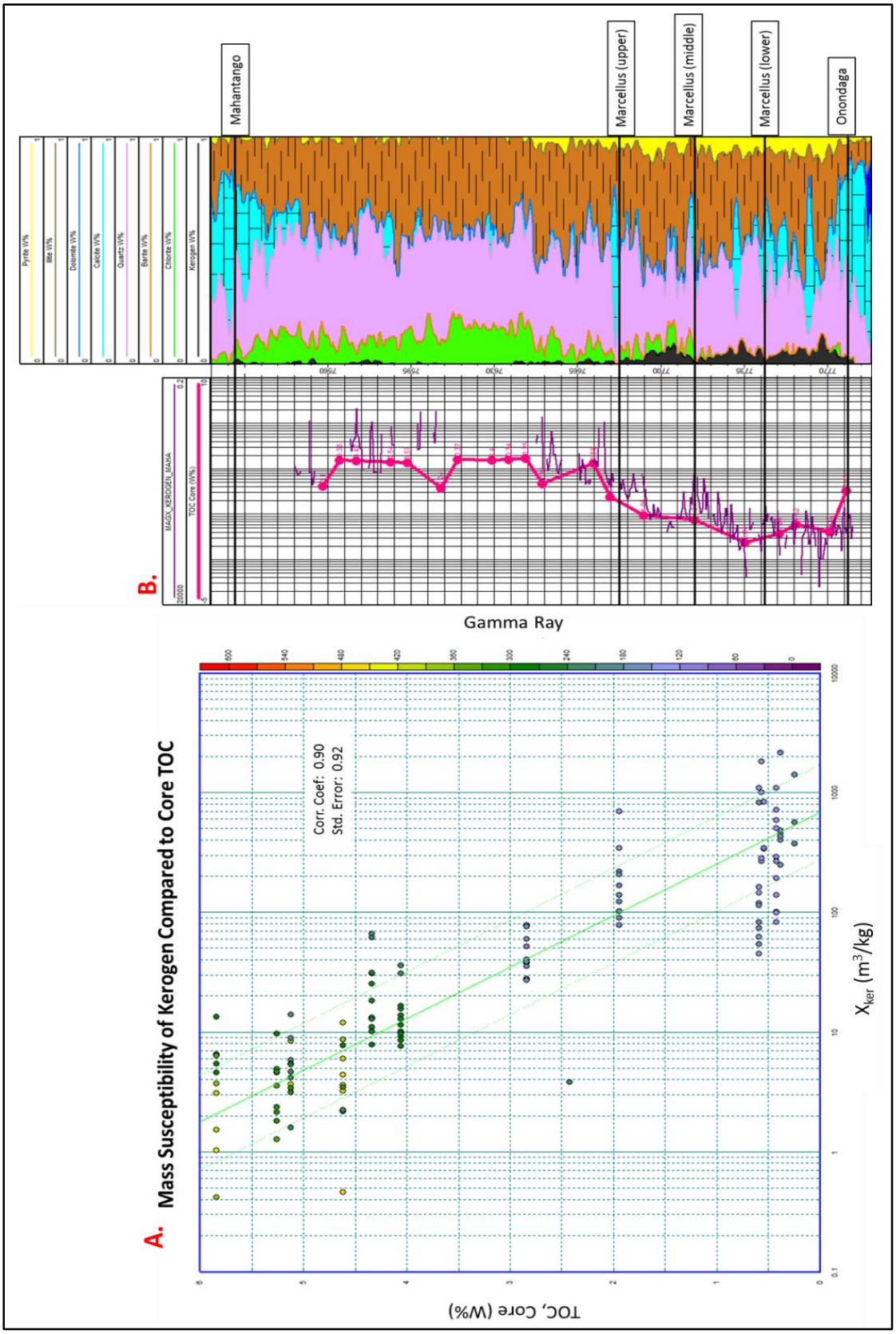

Figure 34. A. Comparison of mass susceptibility of kerogen and TOC derived from the core using Rock-Eval pyrolysis across both formations. The z-axis is gamma ray. **B.** A combination of mass susceptibility of kerogen (purple) and core TOC (pink) on the left and ECS mineralogy curves on the left. Note that the scale for core TOC has been reversed.

When analysis was restricted to the more economically important organic-rich Marcellus Shale, each of the methods used exhibited a lower correlation to core TOC (Table 3). The results of the Schmoker (1993) equation had a correlation coefficient of 0.59 and standard error of 0.73. The results of the Schmoker (1983) equation had a higher correlation coefficient of 0.63 and standard error of 0.70. The ΔlogR method had the lowest correlation coefficient of 0.51 and highest standard error of 0.80. Mass susceptibility of the whole rock produced a correlation coefficient of 0.61 and standard error of 0.73. The isolated mass susceptibility of kerogen retained its logarithmic relationship and produced the highest correlation of 0.69 and lowest standard error of 0.65.

Comparion of Wireline Values to Rock-Eval TOC Estimates (Marcellus Shale Only)		
	Corelation Coefficient	**Standard Error**
Schmoker (93)	0.59	0.73
Schmoker (83)	0.63	0.70
ΔlogR	0.51	0.80
Magnetic Susceptibility (χ_b)	0.61	0.73
Magnetic Susceptibility (χ_{Ker})	0.69	0.65

Table 3. Comparison of analytical methods for deriving TOC from wireline logs and values taken form the core, but restricted to only the Marcellus Shale. Accuracy is shown based upon correlation coefficient and standard error

In an attempt to understand why the mass susceptibility of the kerogen increased so dramatically with depth, it was compared directly to the amount of kerogen present and its level of maturity. The weight percent of kerogen achieved a high correlation coefficient of 0.95 and low standard error of 0.180 (Figure 35), while the vitrinite reflectance values were relatively constant at an average of 1.40% across the entire interval (Table 4). Additionally, comparisons were made against the amount of calcite, quartz, pyrite, illite, dolomite, chlorite, aluminum, calcium, potassium, silicon, sulfur, titanium, gadolinium, and even iron with no discernable patterns.

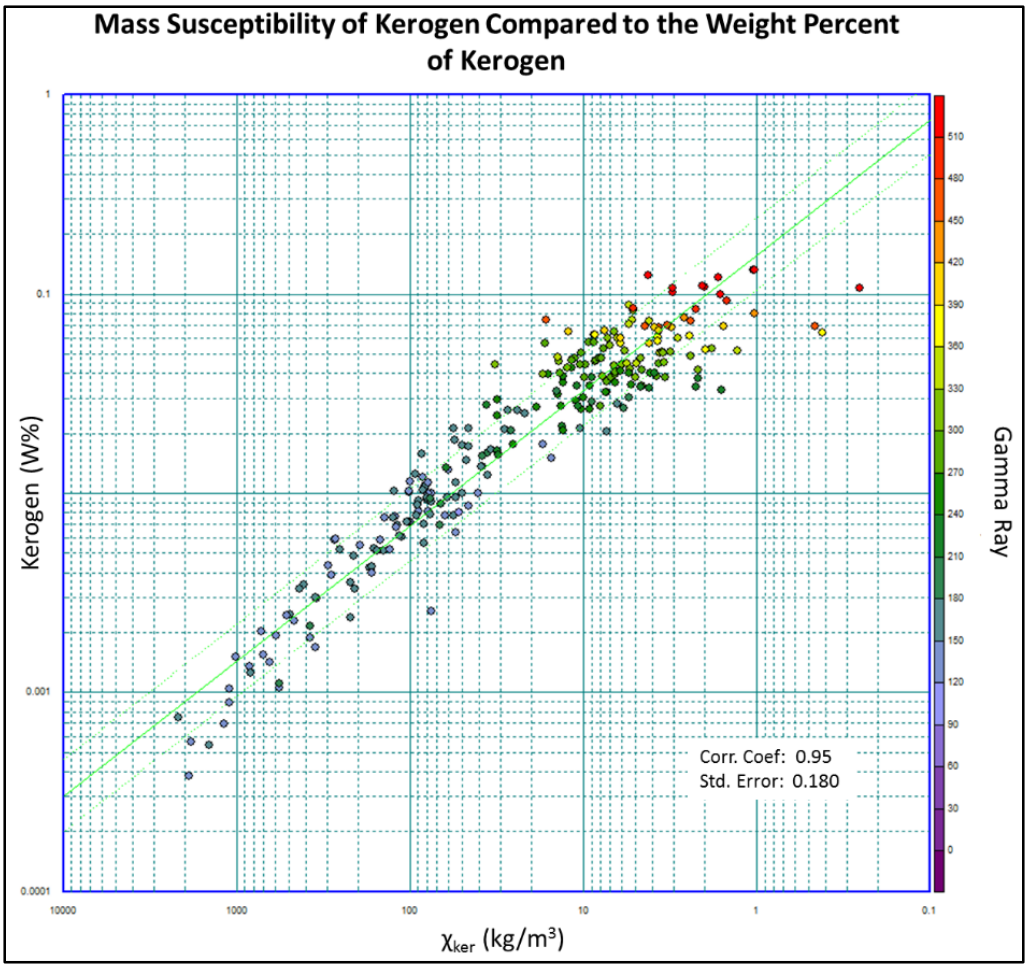

Figure 35. A comparison of the mass susceptibility of kerogen to the weight percent on kerogen across both the Mahantango Formation and the Marcellus Shale. The z-axis is gamma ray.

Vitinite Reflectance Values			
Upper Depth (ft.)	**Vitrinite Reflectance (%)**	**Standard Deviation**	**Count**
7555	1.40	0.06	15
7605	1.38	0.08	14
7655	1.37	0.07	15
7714	1.46	0.07	10
7752	1.40	0.07	15
7765	1.41	0.05	14
Entire Interval	1.40	0.03	83

Table 4. Vitrinite reflectance values by depth. Both formations display a fairly consistent value of 1.40%.

Discussion

Sequence Stratigraphy

The 2nd order T-R cycle recorded within the Middle Devonian shale was easily detected using magnetic susceptibility (Figure 14). Most of the smaller 3rd and 4th order cycles were also recognizable with magnetic susceptibility (Figures 15, 16). However, magnetic susceptibility did not record a 4th order cycle in the middle of the middle Marcellus Shale, nor a 4th order cycle at the top of the upper Marcellus Shale. Conversely, magnetic susceptibility did detect the 4th order cycle in the middle of the Mahantango Formation that occurred between 7598.0' and 7609.5' that was not recognized by the gamma-density method.

The point that the gamma-density method recorded events in the Marcellus shale that the magnetic susceptibility method did not, and that the magnetic susceptibility method recorded events in the Mahantango Formation that the gamma-density method did not should be noticed. Since the gamma readings are so high and density readings so low in the Marcellus Shale relative to the Mahantango Formation above, it enables smaller variations in the rock to exhibit larger effects in the data. The relative change in log values between the two units allows for the detection of smaller cycles and produces a more accurate record of events within the Marcellus Shale. The opposite seems to be true for the Mahantango Formation, where the lower gamma ray and density readings do not allow for the expression of smaller events. Here it seems that the magnetic susceptibility method shows more detail. This may be due to the sensitivity of magnetic susceptibility to the presence of paramagnetic grains. Paramagnetic grains are much more susceptible by weight than diamagnetic grains allowing for detection of very small changes in the terrigenous sediment supply (Ellwood, 2000). It is not clear why the gamma-density method failed to detect the 4th order cycle in the Mahantango Formation. This event coincides with a peak in TOC, which should have produced a drop in density, and a rise in gamma.

Brittleness

BI_{min} does roughly follow the 2nd order T-R cycle across both units, but it is distorted by its exponential relationship to density. In relation to sequence stratigraphy, the more brittle sections are in the RST of the Mahantango Formation and the more ductile sections are in the TST of the Marcellus Shale (Figure 20). This trend is carried over on a smaller scale as well. When analyzed from the top of the Mahantango Formation to the top of the high gamma area in the lower section of the Mahantango Formation, the brittle-ductile couplets of BI_{min} correspond closely to the T-R cycles identified by the magnetic susceptibility method (Figure 21). It was expected that the more brittle quartz grains would increase during regression and the more ductile illite grains would increase during transgression resulting in corresponding variations in brittleness. This was found to be the case as the more brittle sections correspond to the MRS at the top of the RST and the more ductile sections correspond to the MFS at the top of the TST. BI_{min} detects the 4th order cycle that the gamma-density method missed. However, there are two 4th order T-R cycles detected in BI_{min} that were not detected by magnetic susceptibility at ~7630' and ~7615'. Although, this is not necessarily evidence against the correlation. This particular section of the core was missing two pieces at these depths due to previous research and was not analyzed for susceptibility. The T-R cycles from the gamma-density method display weak correlation to BI_{min} in the Mahantango Formation, but they fail to detect many of the 4th order cycles.

When the core was analyzed from the top of the lower Mahantango Formation to the bottom of the Marcellus Shale, there was very good agreement between variations in BI_{min} and the sequence stratigraphic frameworks derived from both the gamma-density method and the magnetic susceptibility method (Figure 22). The brittle-ductile couplets correspond to changes in the sequence stratigraphy, with the more brittle sections corresponding to the MRSs at the top of the RSTs and the more ductile sections corresponding to the MFSs at the top of the TSTs. Here BI_{min} failed to detect any of the 4th order cycles detected in either of the two methods tested. This failure may be a result of the suppression of variations in the data due to the large amounts of TOC.

BI_{el} showed no correlation when compared to either of the units (figures 14, 26, 27). The cause of this discrepancy is evident when the results of BI_{min} and BI_{el} are compared (Figures

28, 29). Since they showed no relation to one another, it's not surprising that they do not show the same relationship to variations in either sequence stratigraphy or magnetic susceptibility. Since they are supposed to measure the same thing, this leaves only two possibilities: one method is correct or neither method is correct. The truth as to which is the case is beyond the scope of this study and should elicit caution when relying upon them.

Organic Carbon

Of the methods tested for estimating the amount of TOC across the two units, the ΔlogR method performed the worst. It had the lowest correlation to core TOC with the highest standard error. While this method has been known to be useful in other plays, the reason it under performs in the Armstrong well is most likely due to the high amounts of pyrite (Figure 12). The low resistivity of pyrite lowers the overall resistivity of the rock resulting in a reduced ΔlogR value. This results in a lower estimation of TOC. The two Schmoker equations performed better, with the 1993 equation outperforming the 1983 equation, which was closer to the ΔlogR method. This discrepancy is not entirely unexpected. Both equations measure TOC with the same method with the only real difference between them being the constants. The 1983 equation was designed for use in the Williston basin and the 1993 equation was designed for the western part of the Appalachian basin. Both the mass susceptibility of the of the whole rock (X_b) and the mass susceptibility of kerogen (X_{ker}) had better correlations to core TOC than traditional methods with X_b preforming only slightly better with a linear relationship and X_{ker} preforming significantly better with a logarithmic relationship (Table 2).

The reasons for the relationship of magnetic susceptibility to TOC is linked to the logarithmic decrease of X_{ker} held. Since both maturity and composition can affect the magnetic susceptibility of a substance, each was analyzed in turn (Hunt, Banerjee, & Moskowitz, 1995). Variations in maturity were ruled out since the burial histories of both units are relatively the same and, more empirically, the vitrinite reflectance values across both units deviated very little from 1.40% (Table 4). This leaves composition as the most likely factor for this increase. Unfortunately for this study, research on the composition of kerogen in these units is still

ongoing and as of this writing is still unknown. However, it is known that the composition of kerogen is not stable from one basin to another and may not even be stable within the same formation. The composition of kerogen is based upon source material. Further, a very strong logarithmic relationship between the weight percent of kerogen and the magnetic susceptibility of kerogen was observed (Figure 35). The magnetic susceptibility of paramagnetic and diamagnetic substances is controlled on the molecular level by the ratio of paired and unpaired electrons and is therefore independent of the quantity of the substance (Mulay, 1963). If the composition of the kerogen is consistent, then the magnetic susceptibility would also be consistent. Because the magnetic susceptibility of the kerogen increases along with the amount of kerogen, then amount of kerogen present can be linked to the sources of the kerogen. This suggests that the areas with the greater amounts of kerogen were sourced from organic material that deposited more diamagnetic material and areas of lesser amounts of kerogen were sourced from organic material that deposited more paramagnetic material. It has been suggested that increases in the amount of TOC within the Marcellus Shale are due to episodic algal blooms (Wrightstone, 2011). Using this hypothesis, it would be reasonable to assume that organisms that are present during the normal habitat of the basin are producing a paramagnetic base level of sediment. During episodes of algal blooms, a large amount of diamagnetic sediment is deposited and the magnetic susceptibility of the base level is lowered as a result. It may also be that the presence of algal blooms displace organisms normally present resulting in further lowering the magnetic susceptibility. This would account for the relationship between the amount of kerogen and its susceptibility. When more is known about the composition of kerogen in this area, it may be possible to establish a stronger link, more tightly constrain the sources, and develop improved methods of predicting TOC.

Conclusions

On the whole, magnetic susceptibility has been shown to be as effective in detecting T-R cycles as the traditional gamma-density method. While it detected less detail in the Marcellus Shale

due to a greater influence of both gamma ray and density values, it detected more detail in the Mahantango Formation where these effects do not occur. Additionally, multiple lines of evidence are provided to support conclusions based upon sequence stratigraphy by using both techniques together.

Variations in BI_{min} showed good correlation to the sequence stratigraphy produced by both methods with brittle-ductile couplets corresponding to regression and transgression respectfully. BI_{el} showed no correlation to either sequence stratigraphic method. Further, it did not even correlate to BI_{min}. This fundamental disagreement between the two methods used for calculating brittleness casts doubt on their effectiveness. More research is needed to determine if either of these methods actually measures the tendency of these units to fracture.

Magnetic susceptibility correlates better to the weight percent of TOC present than does the most commonly used wireline techniques. This is especially true when the mass susceptibility of kerogen is isolated and compared. Though these are only correlations with the most likely scenario being that variations in magnetic susceptibility are linked to the source material and it is the source material that is linked to the amount. Further, evidence was found based upon the relationship of the weight percent of TOC present and the magnetic susceptibility of the TOC, that supports the interpretation of algal blooms as the origin of the high levels of TOC in the Marcellus Shale and that these blooms produced large amounts of diamagnetic sediment that lowered the overall magnetic susceptibility. This method may prove useful in future analysis if this link is found to be present in other parts of the basin and further if it is found in other basins. Even without knowing the kerogen composition, if this relationship holds laterally within the basin, and more data are collected on it, a best fit equation can be generated that can then be used to predict TOC in future exploratory efforts. It would also be expected that, once the composition of kerogen in the Mahantango Formation and Marcellus Shale is discovered, a more direct link could be established that will increase the accuracy of detecting TOC through magnetic susceptibility.

It has been shown that magnetic susceptibility is as accurate at predicting T-R cycles and more accurate at predicting TOC than traditional analytical methods. Further, individual measurements are made accurately and within seconds. The technique is nondestructive, has a

resolution on the scale of centimeters, and the required equipment is inexpensive. These techniques were easily implemented in this study on a shale core, but it could very easily be incorporated into a mud logger's laboratory on a drill site and used to provide near real time data. If the technology can be incorporated in to the bottom hole assembly it could provide real time data on sequence stratigraphy and TOC.

References Cited

Castle, J. (2001). Appalachian basin stratigraphic response to convergent-margin structural evolution. *Basin Research*(13), 397-418.

Catuneanu, O. (2002). Sequence stratigraphy of clastic systems: concepts, merits, and pitfalls. *Journal of African Earth Sciences, 35*(1), 1-43.

Creaney, S., & Passey, Q. (1993). Recurring Patterns of Total Organic Carbon and Source Rock Quality within a Sequence Stratigraphic Framework. *AAPG Bulletin, 77*(3), 386-401.

Crick, R. E., Elwood, B. B., El Hassani, A., Feist, R., & Hladil, J. (1997, September). MagnetoSusceptibility Event and Cyclostratigraphy (MSEC) of the Eifelian-Givetian GSSP and associated boundary sequences in north Africa and Europe. *Episodes, 20*(3), 167-175.

Ellwood, B. (2000, December). Magnetosusceptibility event and cyclostratigraphy method applied to marine rocks: Detrital input versus carbonate productivity. *Geology, 28*(12), 1135-1138.

Ellwood, B. (2001, July). Global correlation using magnetic susceptibilty data from Lower Devonian rocks. *Geology, 29*(7), 583-586.

Ellwood, B. (2013a). Testing high resolution magnetic susceptibility and gamma radiation methods in the Cenomanian-Turonian upper Cretaceous GSSP and neat-by coeval section. *Paleogeography, Paleoclimatology, Paleoecology*(378), 75-90.

Ellwood, B. (2013b). magentostratigraphy susceptibility for teh Quadalupian series GSSP's in Guadalupe Mountains national Park and adjacent areas in west Texas. *Magnetic methods and teh Timing of Geological Processes*, 375-394.

Ettensohn, F., & Barron, L. (1981). *Depositional model for teh Devonian-Mississippian balck-shale sequence of North America: A tectono-climatic approach.* Morgantown, West Virginia, U.S.A.: Uninted States Department of Energy.

Grieser, B., & Bray, J. (2007). Identification of Production Potential in Unconventional Reservoirs. *SPE Production and Operations Symposium*, (p. SPE 106623). Oklahoma City.

Hunt, C. P., Banerjee, S. K., & Moskowitz, B. M. (1995). Magnetic Properties of Rocks ans Minerals. In *Rock Physics and Phase Relations, A Handbook of Physical Constants* (Vol. AGU Refernce Shelf 3, pp. 189-204). American Geophysical Union.

Lash, G., & Engelder, T. (2009, September 4). Thickness trends and sequence stratigraphy of the Middle Devonian Marcellus Formation, Appalachian Basin: Implications for Acadian foreland basin evolution. *AAPG Bulletin, 95*(1), 61-103.

Milici, R., & Swezey, C. (2006). *Assessment of Appalachian Basin Oil and Gas .* USGS. Retrieved 2014, from United States Geological Survey: http://pubs.usgs.gov/of/2006/1237/of2006-1237.pdf

Mulay, L. N. (1963). *Magnetic Susceptibility.* New York: John Wiley & Sons.

Nagata, T. (1961). *Rock Magnetism.* Tokyo: Maruzen Company Ltd.

Passey, Q. R. (1990). A Practical Model for Organic Richness from Porosity and Resistivity Logs. *AAPG Bulliten V.47, No.12*, 1777-1794.

Passey, Q. R. (2010). From Oil-Prone Source Rock to Gas-Producing Shale Reservoir-Geologic adn Petrophysical Characterization of Unconventional Shale-Gas Reservoirs. *SPE 131350*.

Perez, R., & Marfurt, K. (2013, November 11). Calibration of Brittleness to Elastic Rock Properties via Minerology Logs in Unconventional Reservoirs. *AAPG, Search and Discovery Article #41237*.

Rochette, P. (1992). Rock magnetism and the interpretation of anisotropy of magnetic susceptibility. *Reveiw of Geophysics, 30*(3), 209-226.

Schmoker, J. W. (1993). Use of Formation-Density Logs to Determine Organic-Carbon Content in Devonian Shales of the Western Appalachian Basin and an Additional Example Based on the Bakken Formation of the Williston Basin. *USGS Bulletin (1909)*, J1-J14.

Scmoker, J. A., & Hester, T. C. (1983, December). Organic Carbon in Bakken Formation, United States Portion of Williston Basin. *Tha American Association of Petroleum Geologists Bulletin, 67*(12), 2165-2174.

Slatt, R. (2014). Sequence stratigraphy, geomechanics, microsiesmicity, and geochemistry relationships in unconventional resource shales. *Unconventional Resources Technology Conference*, *Search and Discovery Article #80407.* Denver.

Slatt, R., & Abousleiman, Y. (2011, March). Merging sequence stratigraphy and geomechanics for unconventional gas shales. *The Leading Edge*, pp. 274-282.

Wang, F. P., & Gale, J. F. (2009). Screening Criteria for Shale-Gas Systems. *Gulf Coast Association of Geological Societies and the Gulf Coast Section of the Society of Economic Paleontologists and Mineralogists*, 779-793.

Whalen, M., & Day, J. (2008). Magnetic susceptibility, biostratigraphy, and sequence stratigraphy: Insights into Devonian carbonat platform developmentand basin infilling, western Alberta, Canada. *Society for Sedimentary Geology Special Publication*(89), 291-314.

Wrightstone, G. R. (2011). Bloomin Algae! How plaeogeogrphy and algal blooms may have signifigantly impacted deposition and preservation of the Marcellus Shale. *GSA Abstracts with Programs*, *43.*

Zhang, S. (2000, June). Magnetic susceptibility variations of carbonates controlled by sea-level changes. *Science in China, 43*(3).

Appendix

Magnetic Susceptibility Data

Depth	Mag Susceptibility	Depth	Mag Susceptibility	Depth	Mag Susceptibility
7783.3	0.0000918	7761.5	0.0000343	7737.0	0.0000628
7783.2	0.0001660	7761.0	0.0001310	7736.5	0.0000945
7783.0	0.0001320	7760.5	0.0000068	7736.0	0.0000259
7782.7	0.0001430	7760.0	0.0001090	7735.6	0.0000506
7782.5	0.0001680	7759.5	-0.0000005	7735.0	0.0000552
7782.0	0.0000903	7759.0	0.0000287	7734.0	0.0000655
7781.5	0.0001500	7758.6	0.0000589	7733.0	0.0000590
7781.0	0.0002400	7758.0	0.0000669	7732.5	0.0000661
7780.5	0.0001190	7757.5	0.0001390	7732.0	0.0000552
7780.0	0.0000852	7757.0	0.0000476	7731.5	0.0000473
7779.5	0.0001050	7756.5	0.0000205	7731.0	0.0001360
7779.0	0.0000989	7756.0	0.0000228	7730.0	0.0000066
7778.5	0.0000560	7755.5	0.0000984	7730.0	0.0000482
7778.0	0.0000695	7755.0	0.0001970	7729.5	0.0000197
7777.5	0.0000316	7754.5	0.0000780	7729.0	0.0000332
7777.0	0.0000435	7753.8	0.0000563	7728.5	0.0000757
7776.5	0.0000441	7753.5	0.0000581	7728.0	0.0000551
7776.0	0.0000515	7753.0	0.0000081	7727.5	0.0000525
7775.5	0.0001440	7751.0	0.0000917	7727.0	0.0000392
7775.0	0.0001030	7750.5	0.0000575	7726.5	0.0000482
7774.7	0.0000277	7750.0	0.0000232	7726.0	0.0000804
7773.0	0.0000306	7749.5	0.0000937	7725.6	0.0000425
7772.5	0.0000242	7749.0	0.0000398	7725.0	0.0000397
7772.0	0.0000141	7748.5	0.0000483	7724.5	0.0000428
7771.5	-0.0000257	7748.0	0.0000559	7724.0	0.0001230
7771.0	0.0000417	7774.5	0.0000485	7723.5	0.0003030
7770.5	0.0000479	7747.0	0.0000458	7723.0	0.0000432
7770.0	0.0000381	7746.5	0.0000310	7722.0	0.0000724
7769.5	0.0001230	7746.0	0.0000246	7721.5	0.0001520
7769.0	0.0000128	7744.0	0.0000170	7721.0	0.0001880
7768.5	0.0000415	7743.5	0.0000396	7720.5	0.0000619
7768.0	0.0000401	7743.0	0.0001340	7720.0	0.0000883
7767.5	0.0000432	7742.5	-0.0000219	7719.5	0.0000317
7767.0	0.0001270	7742.0	0.0000763	7719.0	0.0000454
7766.5	0.0000613	7741.5	0.0000320	7718.5	0.0000876
7766.0	0.0000571	7741.0	0.0000460	7718.0	0.0002070
7765.3	0.0000327	7740.5	0.0000784	7717.5	0.0003670
7764.0	0.0000377	7740.0	0.0000597	7717.0	0.0000555
7763.5	0.0000465	7739.0	0.0000740	7716.5	0.0000672
7763.0	0.0000796	7738.5	0.0000386	7716.0	0.0000663
7762.5	0.0000494	7738.0	0.0000616	7715.5	0.0000814
7762.0	0.0000335	7737.5	0.0000579	7715.0	0.0000662

Depth	Mag Susceptibility	Depth	Mag Susceptibility	Depth	Mag Susceptibility
7714.5	0.0000575	7690.5	0.0001280	7667.5	0.0002750
7713.0	0.0000572	7690.0	0.0001360	7667.0	0.0001870
7712.5	0.0002000	7689.5	0.0001040	7666.5	0.0002120
7712.0	0.0000694	7689.0	0.0001400	7666.0	0.0002230
7711.5	0.0001250	7688.5	0.0001290	7665.5	0.0001730
7711.0	0.0002150	7688.0	0.0001430	7665.0	0.0001810
7710.5	0.0000751	7687.5	0.0002880	7664.0	0.0002090
7710.0	0.0000692	7687.0	0.0001360	7663.5	0.0002100
7709.5	0.0000837	7686.5	0.0001430	7663.0	0.0003120
7709.0	0.0001280	7686.0	0.0001830	7662.5	0.0002640
7708.5	0.0001160	7684.0	0.0001600	7662.0	0.0001810
7708.0	0.0001180	7683.5	0.0001350	7661.5	0.0001950
7707.5	0.0000621	7683.0	0.0001200	7661.0	0.0001810
7707.0	0.0000521	7682.5	0.0001530	7660.5	0.0001880
7706.5	0.0000929	7682.0	0.0002320	7660.0	0.0002130
7706.0	0.0000810	7681.5	0.0001180	7659.5	0.0001120
7705.5	0.0001670	7681.0	0.0001670	7659.0	0.0002080
7705.0	0.0000618	7680.5	0.0001440	7658.5	0.0002850
7704.0	0.0000870	7680.0	0.0001400	7658.0	0.0002710
7703.5	0.0000964	7679.5	0.0001450	7657.6	0.0002020
7703.0	0.0000954	7679.0	0.0001920	7657.0	0.0003130
7702.5	0.0002450	7678.5	0.0001480	7656.5	0.0002510
7702.0	0.0001340	7678.0	0.0001380	7656.0	0.0002630
7701.5	0.0001410	7677.5	0.0001530	7654.0	0.0001750
7701.0	0.0000998	7677.0	0.0001160	7653.5	0.0002430
7700.5	0.0001020	7676.5	0.0001380	7653.0	0.0001980
7700.0	0.0001210	7676.0	0.0001590	7652.5	0.0002480
7699.5	0.0001000	7675.5	0.0001190	7652.0	0.0002090
7699.5	0.0001070	7674.5	0.0001470	7651.5	0.0002240
7698.6	0.0001270	7674.0	0.0001730	7651.0	0.0003320
7698.0	0.0001100	7673.5	0.0001170	7650.5	0.0001940
7697.5	0.0001010	7673.0	0.0002380	7650.0	0.0002090
7697.0	0.0001120	7672.5	0.0001090	7649.5	0.0002480
7696.5	0.0001110	7672.0	0.0001270	7649.0	0.0002700
7696.0	0.0001040	7671.5	0.0001030	7648.5	0.0001830
7695.5	0.0000772	7671.0	0.0001360	7648.0	0.0001600
7693.5	0.0001360	7670.5	0.0001790	7647.5	0.0002970
7693.0	0.0001000	7670.0	0.0001230	7647.0	0.0001430
7692.5	0.0001280	7669.5	0.0003000	7646.5	0.0001940
7692.0	0.0001130	7669.0	0.0001960	7646.0	0.0001870
7691.5	0.0001230	7668.5	0.0001540	7645.5	0.0001900
7691.0	0.0002380	7668.0	0.0001480	7644.0	0.0001940

Depth	Mag Susceptibility	Depth	Mag Susceptibility	Depth	Mag Susceptibility
7643.5	0.0002140	7620.5	0.0003610	7598.5	0.0002460
7643.0	0.0001690	7620.0	0.0003560	7598.0	0.0002480
7642.5	0.0002260	7619.5	0.0003620	7597.5	0.0002340
7642.0	-0.0001490	7619.0	0.0003600	7597.0	0.0002360
7641.5	0.0001690	7618.5	0.0003500	7596.5	0.0002260
7641.0	0.0002170	7618.0	0.0003450	7596.0	0.0002820
7640.5	0.0002710	7617.5	0.0003640	7595.5	0.0002850
7640.0	0.0002680	7617.0	0.0003980	7595.0	0.0003020
7636.5	0.0002880	7616.5	0.0004930	7594.5	0.0004380
7639.0	0.0004320	7616.0	0.0004190	7594.0	0.0004220
7638.5	0.0003240	7615.0	0.0004490	7593.0	0.0003800
7638.0	0.0003290	7614.5	0.0003830	7592.5	0.0003870
7637.5	0.0002900	7614.0	0.0003830	7592.0	0.0002730
7637.0	0.0002970	7613.6	0.0004230	7591.5	0.0002220
7636.5	0.0002680	7613.0	0.0004160	7591.0	0.0002810
7631.0	0.0003020	7612.6	0.0003130	7590.5	0.0003400
7635.0	0.0002670	7612.0	0.0003160	7590.0	0.0003000
7634.5	0.0002960	7611.5	0.0004960	7589.5	0.0003000
7634.0	0.0002840	7611.0	0.0003240	7589.0	0.0004140
7633.5	0.0003920	7610.5	0.0003890	7588.5	0.0002850
7633.0	0.0003640	7610.0	0.0003670	7588.0	0.0002880
7632.5	0.0003550	7609.5	0.0003400	7587.5	0.0002950
7632.0	0.0003270	7609.0	0.0004270	7587.0	0.0003720
7631.5	0.0003230	7608.5	0.0003730	7586.5	0.0002610
7631.0	0.0004280	7608.0	0.0003490	7586.0	0.0002670
7630.5	0.0003530	7607.5	0.0003830	7585.0	0.0002440
7630.0	0.0003240	7607.0	0.0004600	7584.0	0.0002900
7629.5	0.0003770	7606.5	0.0003240	7583.5	0.0002700
7629.0	0.0002420	7606.0	0.0003610	7583.0	0.0003370
7628.5	0.0003300	7605.5	0.0004870	7582.5	0.0002740
7628.0	0.0003140	7605.0	0.0001590	7582.0	0.0002020
7627.5	0.0003360	7604.0	0.0001950	7581.0	0.0002680
7627.0	0.0004420	7603.5	0.0002660	7580.5	0.0001800
7626.5	0.0003760	7603.0	0.0002040	7580.0	0.0002060
7625.5	0.0003510	7602.5	0.0001930	7579.5	0.0001630
7624.0	0.0003240	7602.0	0.0001970	7579.0	0.0001530
7623.5	0.0003560	7601.5	0.0001960	7578.5	0.0002290
7623.0	0.0003180	7601.0	0.0002480	7758.0	0.0002030
7622.5	0.0003550	7600.5	0.0002140	7577.5	0.0002330
7622.0	0.0003510	7600.0	0.0002180	7577.0	0.0003070
7621.5	0.0003580	7599.6	0.0002050	7576.5	0.0002360
7621.0	0.0004100	7599.0	0.0002020	7576.0	0.0002840

Depth	Mag Susceptibility	Depth	Mag Susceptibility
7575.5	0.0002630	7550.5	0.0002450
7575.0	0.0003950	7550.0	0.0002630
7574.5	0.0002800	7549.5	0.0002490
7574.0	0.0003010	7549.0	0.0003260
7573.0	0.0002680	7548.5	0.0002770
7572.0	0.0002790	7548.0	0.0002760
7571.5	0.0002710	7547.5	0.0001940
7571.0	0.0004210	7547.0	0.0002130
7570.5	0.0003370	7546.5	0.0002040
7570.0	0.0003370	7546.0	0.0001710
7569.5	0.0003080	7545.5	0.0001950
7569.0	0.0004280	7545.0	0.0002530
7568.5	0.0003160		
7568.0	0.0003950		
7567.5	0.0003910		
7567.0	0.0003540		
7566.5	0.0002870		
7566.0	0.0003650		
7565.5	0.0003340		
7565.0	0.0002860		
7564.0	0.0003100		
7562.5	0.0003430		
7562.0	0.0003200		
7561.5	0.0003120		
7561.0	0.0003240		
7560.5	0.0003130		
7560.0	0.0003460		
7559.6	0.0002360		
7559.0	0.0002760		
7558.6	0.0002660		
7558.0	0.0002180		
7557.5	0.0002420		
7557.0	0.0002330		
7556.5	0.0001830		
7556.0	0.0002750		
7555.0	0.0002700		
7553.5	0.0002140		
7553.0	0.0002180		
7552.5	0.0002510		
7552.0	0.0003460		
7551.5	0.0002250		
7551.0	0.0002180		